The dualistic role of the purinergic P2Y12-receptor in an in vivo model of Parkinson's disease: Signalling pathway and novel therapeutic targets

András Iring [a], Adrián Tóth [a,b,c], Mária Baranyi [a], Lilla Otrokocsi [a], László V. Módis [d], Flóra Gölöncsér [a], Bernadett Varga [a,b], Tibor Hortobágyi [d,e,f,g], Dániel Bereczki [c], Ádám Dénes [h], Beáta Sperlágh [a,b,*]

[a] Laboratory of Molecular Pharmacology, Institute of Experimental Medicine, 1083 Budapest, Hungary
[b] János Szentágothai School of Neurosciences, Semmelweis University School of Ph.D. Studies, 1085 Budapest, Hungary
[c] Department of Neurology, Faculty of Medicine, Semmelweis University, 1083 Budapest, Hungary
[d] MTA-DE Cerebrovascular and Neurodegenerative Research Group, Department of Neurology, University of Debrecen, 4032 Debrecen, Hungary
[e] Institute of Pathology, Faculty of Medicine, University of Szeged, 6725 Szeged, Hungary
[f] Department of Old Age Psychiatry, Institute of Psychiatry Psychology and Neuroscience, King's College London, London SE5 8AF, UK
[g] Centre for Age-Related Medicine, SESAM, Stavanger University Hospital, 4011 Stavanger, Norway
[h] Momentum Laboratory of Neuroimmunology, Institute of Experimental Medicine, 1083 Budapest, Hungary

ARTICLE INFO

ABSTRACT

Parkinson's disease (PD) is a chronic, progressive neurodegenerative condition; characterized with the degeneration of the nigrostriatal dopaminergic pathway and neuroinflammation. During PD progression, microglia, the resident immune cells in the central nervous system (CNS) display altered activity, but their role in maintaining PD development has remained unclear to date. The purinergic P2Y$_{12}$-receptor (P2Y$_{12}$R), which is expressed on the microglia in the CNS has been shown to regulate microglial activity and responses; however, the function of the P2Y$_{12}$R in PD is unknown. Here we show that MPTP-induced PD symptoms in mice are associated with marked neuroinflammatory changes and P2Y$_{12}$R contribute to the activation of microglia and progression of the disease. Surprisingly, while pharmacological or genetic targeting of the P2Y$_{12}$R augments acute mortality in MPTP-treated mice, these interventions protect against the neurodegenerative cell loss and the development of neuroinflammation in vivo. Pharmacological inhibition of receptors during disease development reverses the symptoms of PD and halts disease progression. We found that P2Y$_{12}$R regulates ROCK and p38 MAPK activity and control cytokine production. Our principal finding is that the receptor has a dualistic role in PD: functional P2Y$_{12}$Rs are essential to initiate a protective inflammatory response, since the lack of the receptor leads to reduced survival; however, at later stages of neurodegeneration, P2Y$_{12}$Rs are apparently responsible for maintaining the activated state of microglia and stimulating pro-inflammatory cytokine response. Understanding protective and detrimental P2Y$_{12}$R-mediated actions in the CNS may reveal novel approaches to control neuroinflammation and modify disease progression in PD.

1. Introduction

Parkinson's disease (PD) is a chronic, progressive neurodegenerative

disease [1]. The incidence of new Parkinson's cases ranges from 5 to 15 in 100,000 annually [2], most prominently during the sixth to ninth decades of life. PD patients suffer debilitating symptoms that reduce the

quality of life and present increased mortality risks [3,4]; symptoms that include motor function impairments, such as asymmetric tremor, cogwheel rigidity, bradykinesia, as well as non-motor features, including constipation, depression and sleep disorder [2]. Characteristic pathological feature of PD is the selective degeneration of dopaminergic neurons in the substantia nigra *pars compacta* and deposition of insoluble α-synuclein. While both genetic and environmental factors influence disease development, they converge on common pathways to induce PD. These pathways include mitochondrial dysfunction, oxidative stress, impaired autophagy, protein aggregation and neuroinflammation [5].

The ADP-sensitive $P2Y_{12}$-receptors ($P2Y_{12}R$) belong to the G-protein coupled subfamily of nucleotide receptors, and are the molecular target site of widely used antithrombotic drugs preventing stroke and myocardial infarction [6]. Whilst the main location of $P2Y_{12}Rs$ in the periphery are platelets, in the central nervous system (CNS) they are primarily expressed by the microglia, allowing the discrimination of microglia from other cells of the myeloid lineage [7,8]. Our previous work implicated $P2Y_{12}R$ in the regulation of different pain modalities, where receptor inhibition decreased pro-inflammatory IL-1β, TNFα and CXCL1 levels [9]. Recently, we have identified novel microglia-neuron somatic interaction sites, where $P2Y_{12}R$ regulates neuronal activation and pathology [10]. Microglia isolated from $P2Y_{12}R$-deficient mice show normal baseline motility, but have impaired polarization, migration or branch extension towards sites of injury [11]. While the involvement of $P2Y_{12}R$ has been explored in certain pathological conditions, the function of the receptor in Parkinson's disease has not been studied yet. Neurodegeneration during PD occurs either through "cell-autonomous" mechanisms or via indirect degeneration caused by interaction with resident glial cells (astrocytes, microglia). Microglia are the primary innate immune cells in the CNS, continually monitoring synaptic activity, clearing apoptotic cells, and reacting to pathological events through complex inflammatory responses [12]. Microglial activation has been implicated in the pathomechanism of PD in humans [13]; however, it is unclear whether microglia are involved in the initiation of dopaminergic cell death in PD or increased microglial activity merely responds to the production of cytokines or damage-associated molecules from degraded neurons. The functional differences between monocyte-derived macrophages and microglia regarding immunoregulatory, cell migratory and phagocytic function [14,15] imply that microglia contribute differently from other myeloid cells to CNS injury and repair.

Presently available treatment options for Parkinson's disease are based on the supplementation of levodopa (3,4-dihydroxy-L-phenylalanine), an intermediate in the dopamine synthesis pathway, and augmented with drugs that enhance the efficiency of levodopa [16]. The shortcoming of these therapies is that the treatment is symptomatic, improving mainly the motor impairments, moreover, has no effect on disease progression. Here we have investigated the involvement of $P2Y_{12}$-receptors in the acute and subchronic experimental models of Parkinsonism. Blockade of $P2Y_{12}R$ acutely augments mortality after MPTP administration, but apparently protects against the neurodegenerative cell loss and hinders neuroinflammation at later phases of neurodegeneration. Pharmacological inhibition of the receptor during disease progression alleviates the PD symptoms by modulating Rho-kinase (ROCK) and p38 MAPK activity and reducing pro- and anti-inflammatory cytokine production. Interestingly, while ROCK-inhibition via fasudil has an apparent protective effect during experimental PD, it also conveys a wide-range of undesirable side-effects that are detrimental during disease resolution. Our findings implicate a pivotal role for $P2Y_{12}R$ in experimentally-induced PD, and we propose the receptor as a promising highly selective and specific pharmacological target to impede disease progression in Parkinson's Disease.

2. Materials and methods

2.1. Animals and treatment

All procedures involving animal care and use in this study were performed in accordance with the Institutional Ethical Codex and the Hungarian Act of Animal Care and Experimentation guidelines (40/2013, II.14), which are in accordance with the European Communities Council Directive of September 22, 2010 (2010/63/EU). The Animal Care and Experimentation Committee of the Institute of Experimental Medicine and the Animal Health and Food Control Station, Budapest, have also approved all experiments (PEI/001/776–6/2015). Experimental animals were treated humanely, all efforts were made to minimise animal suffering and reduce numbers of experimental animals. Animal studies are reported in compliance with the ARRIVE guidelines [17,18]. Animals were housed under a 12-hour light- dark cycle in a temperature- ($23 \pm 2\,°C$) and humidity-controlled room ($60 \pm 10\%$) and had access to food and water ad libitum. All studies in vivo were carried out during the light phase of the cycle. Experiments were performed using wild-type (C57/Bl6N) and *P2ry12* gene-deficient (*P2ry12$^{-/-}$*) male mice aged 8–14 weeks, with an average weight of 27 ± 1.4 gramms. The original breeding pairs of *P2ry12$^{-/-}$* knockout mice, B6;129-P2ry12^{tm1Dgen}/H were obtained from Deltagen Inc. (San Matteo, CA, USA). Cloning and breeding strategy, and genotyping protocol has been described previously [19].

All mice were backcrossed onto a C57BL/6N background at least 8–10 times, and experiments were performed with littermates as controls.

2.2. Treatment protocol

Two different experimental approach was used.

2.2.1. in vivo acute MPTP model

The acute induction of Parkinson's disease was described in detail elsewhere [20]; briefly, animals were randomly assigned into experimental groups. All animals received either intrathecal injection of PSB 0739 (0.3 mg / kg) or saline 18 h prior to MPTP treatment. Intrathecal administration enables the direct administration of small molecules that are otherwise unable to cross the blood-brain barrier to the central nervous system without damaging the spinal cord [21]. Previous studies showed that PSB 0739 can hardly permeate the blood brain barrier due to its chemical character [22], therefore this route of drug administration allowed for the selective targeting of the centrally expressed $P2Y_{12}R$ (ie. expressed on microglia), without influencing the peripherally expressed receptors. MPTP was injected (4×20 mg / kg intraperitoneally) 2 h apart; behavioral tests were performed 6 and 24 h after the first MPTP injection; while animals were sacrificed either 6 and 24 h for the assessment of microglia activation, cell apoptosis and neuron viability; 24 h after the first MPTP injection for the assessment of cytokine levels or 72 h after the initial MPTP-treatment for measurement of biogenic amine content determined by HPLC-EC analysis and for histochemistry. Schematic of the experimental protocol is included in the Supporting Data section (Supplementary Fig. 1A).

2.2.2. in vivo subchronic MPTP model

Animals were treated daily dose of MPTP (20 mg / kg, intraperitoneally) or saline for five consecutive days; in previous studies we have verified that the majority of MPTP is converted to the toxic metabolite MPP^+ by this time point [20]. Subsequently, animals were randomly divided into two groups, receiving daily intrathecal injections of PSB 0739 (0.3 mg / kg) or saline for four consecutive days [20]. Alternatively, animals were treated with daily dose of MPTP (20 mg / kg, intraperitoneally) or saline for five consecutive days, followed by replacing the drinking water containing either fasudil (50 mg / kg body weight per day) or its vehicle for three weeks. Fasudil has the advantage

over Y-27632 (a distinct Rho-kinase inhibitor) that it allows for oral delivery and does not require continuous parenteral administration. Behavioral tests were performed before MPTP administration and 21 days after treatment with PSB 0739, fasudil or its vehicle. Mice were sacrificed 21 days after MPTP treatment complemented with PSB 0739, fasudil or its vehicle treatment, and samples were taken for histo-chemistry and biogenic amine contents analysis. In some cases, the experiment was terminated after the last MPTP treatment and tissues were collected for histochemistry or for the assessment of microglia activation. Schematic of the experimental protocol is included in the Supporting Data section (Supplementary figure 1B and C).

2.3. Behavioral analyses

Rotarod test was performed to assess motor coordination on the IITC (Woodland Hills, CA, USA) Rotarod Apparatus. The modified protocol used was described by Shiotsuki [23]. Briefly, the tests are performed on an 8 cm diameter rotating rod 25 cm above the base of the apparatus rotating with fixed speed (10 rpm) in order to obtain a steep learning curve, consequently this protocol is superior in the assessment of motor skill learning rather than maximal gait performance. Motor coordination of animals was tested for 180 s. Acclimatization to the device was performed for 2 consecutive days before the start of the experiment. Regarding the acute MPTP treatment model, baseline latencies to fall were determined 1 h before drug administration, followed by either PSB 0739 (0.3 mg / kg) treatment or its vehicle. The falling latency was measured at 6 and 24 h after the final MPTP treatment. Regarding the subchronic MPTP model, baseline values were obtained 1 h prior to the start of MPTP treatment or its vehicle on day 1. The latency time to fall was again measured 21 days after the last MPTP administration.

2.4. Tyrosine hydroxylase (TH) immunohistochemistry

Mice were euthanized with gradual filling of CO_2 inhalation and the chest cavity was opened for perfusion with 4 °C phosphate buffered saline (PBS) followed by fixation with 4% PFA at room temperature for 20 min. After fixation brain was carefully removed and cut in the coronal plane with a brain matrix slicer at the region of + 0.74 mm from Bregma [24], followed by 24 h post-fixation in 4% PFA at 4 °C. Subsequently, the sample was sectioned with a sliding microtome (Leica Microsystems Inc., Richmond Hill, ON) at 40 μm thickness starting at 2.46 mm from Bregma and ending at 4.04 mm from Bregma and four series of coronal midbrain sections were collected. A single series of sections were used for immunostaining, where sections were processed together and the same batch of reagents were used. Endogenous peroxidase activity was blocked by 0.3% H_2O_2 in methanol for 20 min. To reduce non-specific binding, Vector blocking solution (2.5% normal horse serum) was applied for 2 h at room temperature. Sections were incubated with anti-tyrosine hydroxylase antibody (Sigma-Aldrich GmbH, Merck KGaA, Darmstadt, Germany, Cat. No. AB152) overnight at 4 °C. Following, the secondary antibody (The ImmPRESS Universal Antibody Kit, anti-mouse/rabbit) and ImmPACT DAB (both purchased from Vector Laboratories, Burlingame, CA) was applied according to the manufacturer's instructions. The sections were dried on glass slides and coverslipped with ProLong™ Gold Antifade Mountant (Thermo Fisher Scientific, Waltham, MA, USA).

2.5. Stereological estimation

Ten randomly selected sections across the entire antero-posterior extent of the substantia nigra, separated by 160 μm (1/4 series), were used for counting as described by Ip et al. [24]. TH-immunoreactive dopaminergic neuronal perikarya were identified by their rounded or ovoid shape and cell size. Parameters used for TH stereological counting were as follows; grid size, 300 μm × 300 μm; counting frame, 50 μm × 50 μm, and 3 μm guard zones. Mean tissue thickness was determined

from three randomly selected counting sites per section using the imaging software (NIS-Elements, Nikon Instruments Inc., Melville, NY, USA). The estimated number of TH-positive cells per animal (N) were calculated using the formula [25]:

$$N = \Sigma Q^- \times \frac{t}{h} \times \frac{1}{asf} \times \frac{1}{ssf}$$

where ΣQ^- is the sum of all TH-positive neurons counted in all optical disectors of one brain section; h is the height of the optical disector; t is the mean tissue thickness of the section; asf is the area sampling fraction defined as the proportion of the area (A) of the optical disector (A optical disector) frame size within the square size of the grid (A x,y step) (A optical disector/A x,y step); ssf is the section sampling fraction defined as the proportion of sections of the whole serially cut brain. The final N values were only included if their coefficient of error (CE) were less than 0.10 [26]. The analysis was performed by a user blinded to group assignment. The n number displayed on the figures and marked in the figure legends signify the number of animals used for the indicated experimental condition.

2.6. Cresyl-violet (Nissl) histochemistry

Mice were euthanized with gradual filling of CO_2 inhalation and the chest cavity was opened for perfusion with 4 °C phosphate buffered saline (PBS) followed by fixation with 4% PFA at room temperature for 20 min. After fixation brain was carefully removed and cut in the coronal plane with a brain matrix slicer at the region of + 0.74 mm from Bregma [24], followed by 24 h post-fixation in 4% PFA at 4 °C. Subsequently, the sample was sectioned with a vibratome at 40 μm thickness starting at 2.46 mm from Bregma and ending at 4.04 mm from Bregma and all coronal midbrain sections were collected. Cresyl-violet staining was performed as described by Paul et al. [27,28]. Briefly, samples were mounted on Menzel SuperFrost Ultra Plus™ slides (Thermo Fisher Scientific) and allowed to dry for 24 h on room temperature. Slides were processed together and the same batch of reagents were used. Samples were demyelinated using increased ethanol containing solutions (2 min each) and Xylene (5 min), followed by the return to aqueous phase (30 s each step). Cresyl-violet staining was performed using 0.1% solution for 3 min. Clearing of the samples was carried out in 50% ethanol for 15 min. Slides were fixed in xylene and mounted overnight with DPX Mounting medium (Sigma-Aldrich GmbH).

2.7. Immunofluorescent labeling and confocal laser imaging

For animal experiments, mice were sacrificed and brain sections have been prepared as described previously. Samples were washed three times with PBS and incubated in PBS containing 5% BSA and 0.3% Triton X-100 for 2 h. Samples were randomly divided into groups and were incubated overnight at 4 °C in the same buffer containing anti-CD68 antibody (1:250), anti-Iba1 antibody (1:500) together with anti-phospho-p38 MAPK (T180/Y182) antibody (1:250). Samples from the same animal were incubated overnight at 4 °C in the same buffer containing anti-Iba1 antibody (1:500) together with anti-p38 MAPK antibody (1:250) to test whether treatment influences the basal expression of p38 MAPK. Next, a second set of experiments were performed to test the acute, time-dependent effect of MPTP administration, where samples were incubated in the same buffer overnight at 4 °C containing anti-CD68 antibody (1:250), anti-Caspase-3 antibody (1:500) together with anti-MAP2 antibody (1:1000). A third set of experiments were performed to test P2Y$_{12}$-receptor expression in the substantia nigra, where samples were incubated overnight at 4 °C in the same buffer containing anti-CD68 antibody (1:250) together with anti-P2Y$_{12}$-receptor antibody (1:1000). To validate the anti-P2Y$_{12}$-receptor antibody specificity, samples from wild-type control and P2Y$_{12}$R-KO mice were harvested and prepared as described. Samples were incubated overnight at 4 °C in

the PBS containing 5% BSA and 0.3% Triton X-100 buffer supplemented with anti-Iba1 antibody (1:500) together with anti-P2Y$_{12}$-receptor antibody (1:1000). After overnight incubation, samples were washed in PBS and incubated with the appropriate AlexaFluor-564 conjugated antibody and AlexaFluor-488 conjugated secondary antibody (Molecular Probes, Thermo Fisher Scientific; 1:200) as well as with Hoechst 33342 (Thermo Fisher Scientific; 1:10000) for 1 h avoiding exposure to light. For cell culture experiments, BV-2 cells were cultured on cover slips placed in cell culture dishes. To visualize microglia activation after ADP treatment, an ectonucleotidase inhibitor, ARL 67156 (30 μM), either combined with PSB 0739 (500 nM) or with its vehicle, was added to the extracellular solution 20 min before the experiment. Following, the medium was replaced, and ADP (100 μM) was added to the solution for 0, 6 or 24 h. After the allotted time, the medium was removed, and the cells were washed with ice-cold PBS, thereafter fixed in 4% PFA at room temperature for 20 min. Following, cells were washed three times with PBS and incubated in PBS containing 5% BSA and 0.3% Triton X-100 for 2 h. Samples were incubated overnight at 4 °C in the same buffer containing anti-CD68 antibody (1:250), anti-Iba1 antibody (1:500) together with anti-phospho p38 MAPK (T180/Y182) antibody (1:250). After overnight incubation, samples were washed in PBS and incubated with the appropriate AlexaFluor-564 conjugated antibody and AlexaFluor-488 conjugated secondary antibody (Molecular Probes, Thermo Fisher Scientific; 1:200) as well as with Hoechst 33342 (Thermo Fisher Scientific; 1:10000) for 1 h avoiding exposure to light. Samples were mounted in ProLong™ Gold Antifade Mountant (Thermo Fisher Scientific) overnight. Immunofluorescent signal was analyzed using a Nikon Eclipse Ti-E inverted microscope (Nikon Instruments Europe B.V., Amsterdam, The Netherlands), and a C2 laser confocal system. Immunofluorescent signal intensity was quantified following the protocol of Shihan et al. [29]. Briefly, during image acquisition, identical laser settings for gain, offset and intensity parameters were used. The acquired pictures were processed in ImageJ Fiji, where initially the background was subtracted for all channels (rolling ball radius: 50 pixels), followed by the automated measurement of mean fluorescent intensity for each channel. Quantitative analysis of immunostaining was performed on at least three, randomly selected fields within the region of interest for each brain section. Three independent brain slices were analysed from each animal.

2.8. HPLC determination of nucleotides, catechol- and indoleamines content

Catechol- and indole amines, nucleotides (ATP, ADP, AMP) and adenosine, in extracts from brain tissue were determined using HPLC method. Mice were decapitated 3 or 21 days after the last MPTP or vehicle treatment, the striatum was dissected on ice and was snap frozen in liquid nitrogen. The tissue was ultrasonically homogenized with 200 μl of ice-cold 0.01 M perchloric acid solution containing theophylline (as an internal standard) at a concentration of 10 μM and 0.5 mM sodium metabisulfite (antioxidant of biogenic amines). The tissue extract was centrifuged at 3510 × g for 10 min at 4 °C and the pellet was saved for protein measurement according to Lowry et al. [30]. Perchloric anion from the supernatant was precipitated by 1 M potassium hydroxide, the precipitate was then removed by centrifugation. The sample extracts were kept at −20 °C until analysis. Quantification of nucleotides and biogenic amines from tissue was performed by online column switching separation. ACE Ultra Core Super 5 μm particle size packed columns from A.C.T.L. (Scotland) were used for analysis. The phenylhexyl packed (7.5 cm × 2.1 mm ID) column was used for online solid phase extraction (SPE). Upon completion of sample enrichment and purification the separation was continued by connecting the analytical C-18 (150 × 2.1 mm) column. The flow rate of the mobile phases ["A" 10 mM potassium phosphate, 0.25 mM EDTA "B" with 0.45 mM octane sulphonyl acid sodium salt, 8% acetonitrile (v/v), 2% methanol (v/v), pH 5.2] was 350 or 450 μl / min, respectively in a step

gradient application [31]. The enrichment and stripping flow rate of buffer [10 mM potassium phosphate, pH 5.2] was during 4 min and the total runtime was 55 min. The HPLC system used was a Shimadzu LC-20 CE Analytical & Measuring Instruments System, with an Agilent 1100 Series Variable Wavelength Detector and BAS CC-4 amperometric detector in a cascade line. The detection of nucleotides and the internal standard (theophylline) was performed at 253 nm wavelengths by UV and biogenic amines were determined electrochemically at an oxidation potential of 0.73 V. Concentrations were calculated by a two-point calibration curve internal standard method: (Ai × f × B)/(C × Di × E) (Ai: Area of nucleotide or biogenic amine component; B: Sample volume; C: Injection volume; Di: Response factor of 1 pmol biogenic amine and 1 nmol nucleotide standard; E: Protein content of sample; f: factor of Internal Standard (IS area in calibration / IS area in actual)). The data were expressed as pmol / mg protein, unless stated otherwise. Statistical analysis was performed using the TIBC Statistical Program to assess normal distribution of all continuous variables and the nonparametric Kolmogorov-Smirnov test was used to test statistical differences. Where the measured variables met the normality assumption, parametric tests were performed. The threshold for statistical significance was set at $p < 0.05$.

2.9. Cytokine measurement

For experiments to measure cytokine levels from brain tissue, samples were collected 24 h after the last intraperitoneal injection of MPTP (20 mg / kg) or saline. Mice were perfused transcardially with 0.1 M phosphate buffered saline (PBS), and substantia nigra and striatum were homogenized in RIPA lysis buffer (150 mM NaCl, 50 mM Tris-HCl (pH 7.4), 5 mM EDTA, 0.1% (w/v) SDS, 0.5% sodium deoxycholate and 1% Triton X-100) supplemented with protease inhibitors [32,33]. After centrifugation (16000 × g for 20 min at 4 °C), supernatants were collected and protein concentration were measured using BCA Protein Assay Kit (Thermo Fisher Scientific, Pierce). For experiments to determine cytokine concentration after ADP administration in cell culture dishes, the murine immortalized microglia cell line (BV-2) was used. In order to prevent rapid degradation of ADP, 30 μM of ARL 67156, either combined with PSB 0739 (500 nM) or with its vehicle, was added to the extracellular solution 20 min before the experiment. Following, the medium was replaced, and ADP (100 μM) was added to the solution for 0, 6 or 24 h. Following the allotted time period, the medium was collected and after a brief centrifugation (700 × g for 5 min at 4 °C), supernatants were collected. The cells from the culture dishes were lysed in RIPA buffer supplemented with protease inhibitors, the insoluble cellular components were pelleted (16000 × g for 20 min at 4 °C) and supernatants were transferred to a new Eppendorf tube. The protein concentration was measured using BCA Protein Assay Kit (Thermo Fisher Scientific, Pierce). Concentration of IL-1β, IL-6, IL-10 and TNFα were measured using BD Cytometric Bead Array Flex Sets (BD Biosciences, San Jose, CA, USA). Measurements were performed on a BD FACSVerse flow cytometer, and data were analyzed using the FCAP Array version 5 software (Soft Flow). Cytokine concentrations of brain tissue or cell culture supernatant were normalized to total protein levels measured. The cytokine levels are expressed as pg / mg total protein, unless stated otherwise.

2.10. Determination of [^{3}H]dopamine release ([^{3}H]DA)

Experiments were performed on young adult (2–3 months) male wild-type and P2Y$_{12}$-receptor knockout (*P2ry12$^{-/-}$*) mice. The [^{3}H]DA release experiments were conducted using the method with slight modifications described in our previous papers [34]. Briefly, the mice were euthanized with gradual filling of CO$_2$ inhalation, and subsequently decapitated. The striatum was dissected in ice-cold Krebs solution saturated with 95% O$_2$ and 5% CO$_2$, sectioned (400-μm-thick slices) using a McIlwain tissue chopper and incubated in 1 ml of modified Krebs

solution (113 mM NaCl, 4.7 mM KCl, 2.5 mM $CaCl_2$, 1.2 mM KH_2PO_4, 1.2 mM $MgSO_4$, 25 mM $NaHCO_3$, and 11.5 mM glucose), pH 7.4, in the presence of 5 μCi/ml [^{3}H]dopamine, (specific activity 60 Ci/mmol; ARC, Saint Louis, MO, USA) for 45 min. The medium was bubbled with 95% O_2 and 5% CO_2 and maintained at 37 °C. After loading, the slices were continuously superfused with 95% O_2 and 5% CO_2-saturated modified Krebs solution (flow rate: 0.7 ml/min). After a 90 min washout period to remove excess radioactivity, perfusate samples were collected over 3 min periods and assayed for tritium content. The temperature was strictly kept at 37 °C. At 6 min after the start of the collection, the slices were subjected to a 3 min perfusion of the Na$^+$-channel activator veratridine (5 μM) and then changed to normal Krebs solution until the end of the collection period. In some experiments, two consecutive veratridine stimulus were applied 30 min apart (S1, S2) and the P2Y$_{12}$R antagonist PSB 0739 (1 μM) was perfused 15 min before the second veratridine stimulation (S2). The effect of PSB 0739 on the veratridine-evoked [^{3}H]DA release was expressed as the ratio of S2 over S1 and compared with control S2/S1 values. The radioactivity released from the preparations was measured using a Packard 1900 Tricarb liquid scintillation spectrometer, using Ultima Gold Scintillation cocktail. The release of tritium was expressed in Bq/g or as a percentage of the amount of radioactivity in the tissue at the sample collection time (fractional release). The tritium uptake in the tissue was determined as the sum of release + the tissue content after the experiment and expressed in Bq/g. For the evaluation of the basal tritium outflow, the fractional release measured in the first 3 min sample under drug free conditions were taken into account. The veratridine-induced [^{3}H]DA efflux calculated as the net release in response to the respective stimulus by subtracting the release before the stimulation from the values measured after stimulation (S1, FRS1).

2.11. Cultured cells

Murine immortalized microglia cell line (BV-2) were cultured in Dulbecco's modified Eagle's medium supplemented with heat inactivated FBS (10%), insulin, non-essential amino acid, penicillin-streptomycin and gentamycin at pH 7.2–7.4 (ThermoFisher Scientific, Cat No. 11966025), and confluent cells at a passage of ten or less were used in experiments.

2.12. Western blotting

Cells were lysed in radioimmunoprecipitation assay (RIPA) buffer containing 150 mM NaCl, 50 mM Tris-HCl (pH 7.4), 5 mM EDTA, 0.1% (w/v) SDS, 0.5% sodium deoxycholate and 1% Triton X-100 as well as protease inhibitors (10 mg / ml leupeptin, pepstatin A, 4-(2-aminoethyl) benzensulfonyl-fluorid and aprotinin) and phosphatase inhibitors (PhosSTOP™, Roche AG, Basel, Switzerland). Total cell lysates were separated by sodium dodecyl sulfate-polyacrylamide gel electrophoresis. Protein was then transferred onto nitrocellulose membranes, followed by overnight incubation with primary antibodies. Membranes were incubated with horseradish peroxidase-conjugated secondary antibodies (Cell Signaling Technology Inc., Danvers, MA, USA) for 1 h room temperature and were developed using the ECL detection system (Thermo Scientific Pierce, Life Technologies). In cases where protein phosphorylation was analyzed using phosphosite-specific antibodies, membranes were first developed with anti-phosphosite-specific antibodies. After evaluation, antibody dissociation from the membrane was induced using Restore™PLUS Western Blot Stripping Buffer (Thermo-Fisher Scientific) according to the manufacturer's instructions, and membranes were then reprobed with antibodies recognizing the corresponding protein. Protein band intensities were analyzed by ImageJ software (NIH). Intensity values of bands representing phosphorylated sites of proteins were normalized to the intensity of the band representing total protein.

2.13. Post-mortem human brain tissue

Human brain tissue was obtained from patients who died from causes linked to Parkinson's disease (ethical approval ETT-TUKEB 62031/2015/EKU, 34/2016 and 31443/2011/EKU [518/PI/11]). Informed consent was obtained for the use of brain tissue and for access to medical records for research purposes, and the use of tissue samples were in accordance with the Declaration of Helsinki. Brains of 2 patients with Parkinson's disease dementia were removed within 3 days after death and immersion fixed in 4% paraformaldehyde. Brain dissection, macroscopic description, regional sampling, tissue processing and staining were done following standard protocols as described in earlier [35] including BrainNet Europe and Brains for Dementia Research UK. Briefly, dissected and paraffin embedded samples from the middle frontal gyrus (Brodmann area 9) and striatum, respectively, were selected for this study, and 7 μm thick sections were cut on a sledge microtome. Sections were routinely de-waxed, blocked for endogenic peroxidase activities in ethanol containing 3% (v/v) H_2O_2 for 30 min, and heat-treated in appropriate antigen retrieval buffer solutions using a household microwave oven (5 min at 800 W, 2 × 5 min at 250 W). Non-specific epitopes were blocked with 1% (v/v) bovine serum albumin dissolved in Tris-buffered saline (TBS pH=7.4) for one hour. The sections were incubated with the primary antibodies in 1:500 concentration overnight at 4 °C. Detection was processed using biotin-free secondary antibodies (MACH 4 Universal HRP-Polymer, Biocare Medical LLC, Pacheco, CA, USA; Cat. No. M4U534). For visualization, 3, 3′-diaminobenzidine tetrahydrochloride (DAB) reagent (Biocare Medical LLC, Cat. No. DB801) was applied. Harris' haematoxylin was used to perform nuclear counterstain. After dehydration the sections were covered with ScienCell medium and Mountex coverslip.

2.14. Reagents

1-methyl-4-phenyl-1,2,3,6-tetrahydropyridine (MPTP, Cat. No. M0896), adenosine 5′-diphosphate (Cat. No. A2754), bovine serum albumin (Cat. No. A2153), lipopolysaccharide (Cat. No. L2880) and veratridine (Cat. No. V5754) were purchased from Sigma-Aldrich. Y-27632 were obtained from Cayman Chemicals, Ann Arbor, Michigan, USA (Cat. No. 129830-38-2). ARL 67156 (Cat. No. 1283) and PSB 0739 were from Tocris Biosciences, Bristol, UK (Cat. No. 3983) and Fasudil-HCl were from LC Laboratories, Woburn, MA, USA (Cat. No. F-4660). Antibodies directed against phosphorylated p38 MAPK (Cat. No. 9211; Lot. No. 25) and p38 MAPK (Cat. No. 9212; Lot. No. 26) were purchased from Cell Signaling Technology, against tyrosine hydroxylase was from Sigma-Aldrich (Cat. No. AB152; Lot. No. 3256647), against P2Y$_{12}$-receptor was from AnaSpec, Fremont, CA, USA (Cat. No. AS-55043A; Lot. No. UB1701), against Iba1 was from Synaptic System GmbH, Göttingen, Germany (Cat. No. 234004; Lot. No. 2–20), against CD68 was purchased from Bio-Rad Laboratories, Hercules, CA, USA (Cat. No. MCA1957). Antibody against MAP2 (Cat. No. ab5392; Lot. No. AB_U77256) was from Abcam plc., Cambridge, UK, and directed against Caspase-3 was from Synaptic System (Cat. No. 236003).

2.15. Experimental design and statistical analyses

Sample size was calculated as described previously [36], and was estimated based on a pilot study of MPTP and vehicle treated mice. Experimental animals were randomly assigned to experimental groups prior to the start of the experiment. Data acquisition and evaluation were performed by investigators blind to the experimental status of the subject. To adhere to the 3 R reduction strategies, experimental mice were used in multiple experiments to reduce the number of experimental animals to the greatest possible extent. Specifically, following the initial set of experiments, surviving mice were randomly assigned to the next set of experiments. The exact number and origin of distinct biological samples taken without applying preselection criteria from experimental

animals are indicated in their respective figures legend. In case of in vivo studies the dose selection was based on previous studies [9,20]. Statistical analysis was performed using the GraphPad Prism software v.6.07 from GraphPad Software Inc. (La Jolla, CA, USA). Values are presented as mean ± SEM; *n* represents the number of independent experiments. Probability distribution of all continuous variables was performed; nonparametric data were analyzed using Kolmogorov-Smirnov test, whereas in case of normally distributed data, statistical analysis between two groups were performed with an unpaired two-tailed Student's *t* test, while multiple group comparisons were analyzed with one-way ANOVA followed by Tukey's post-hoc test, unless stated otherwise, and comparisons between multiple groups at different time points were performed using two-way ANOVA followed by Bonferroni's post-hoc test. A *p* value of less than 0.05 was considered to be statistically significant.

3. Results

3.1. *P2Y$_{12}$-receptor invalidation promotes MPTP induced mortality and modulates the early phase of microglia activation*

First, we investigated the role of P2Y$_{12}$R in the development of Parkinson's disease, utilizing mice with genetic deficiency for the *P2yr12* gene (herein referred to as P2Y$_{12}$R-KO) or using pharmacological blockade by PSB 0739, a specific P2Y$_{12}$R inhibitor [37]. We have observed that genetic deletion or pharmacological blockade of the receptor contributes to lower survival following MPTP-treatment (Fig. 1A and Supplementary Fig. 1A). While the survival rate in wild-type control and P2Y$_{12}$R-KO mice receiving only PSB 0739 was indistinguishable from the vehicle treated control group, MPTP administration contributed to a casualty rate of approximately 25% in wild-type control mice. Remarkably, MPTP treatment combined with dysfunctional P2Y$_{12}$R markedly increased mortality (approximately 41% in wild-type PSB
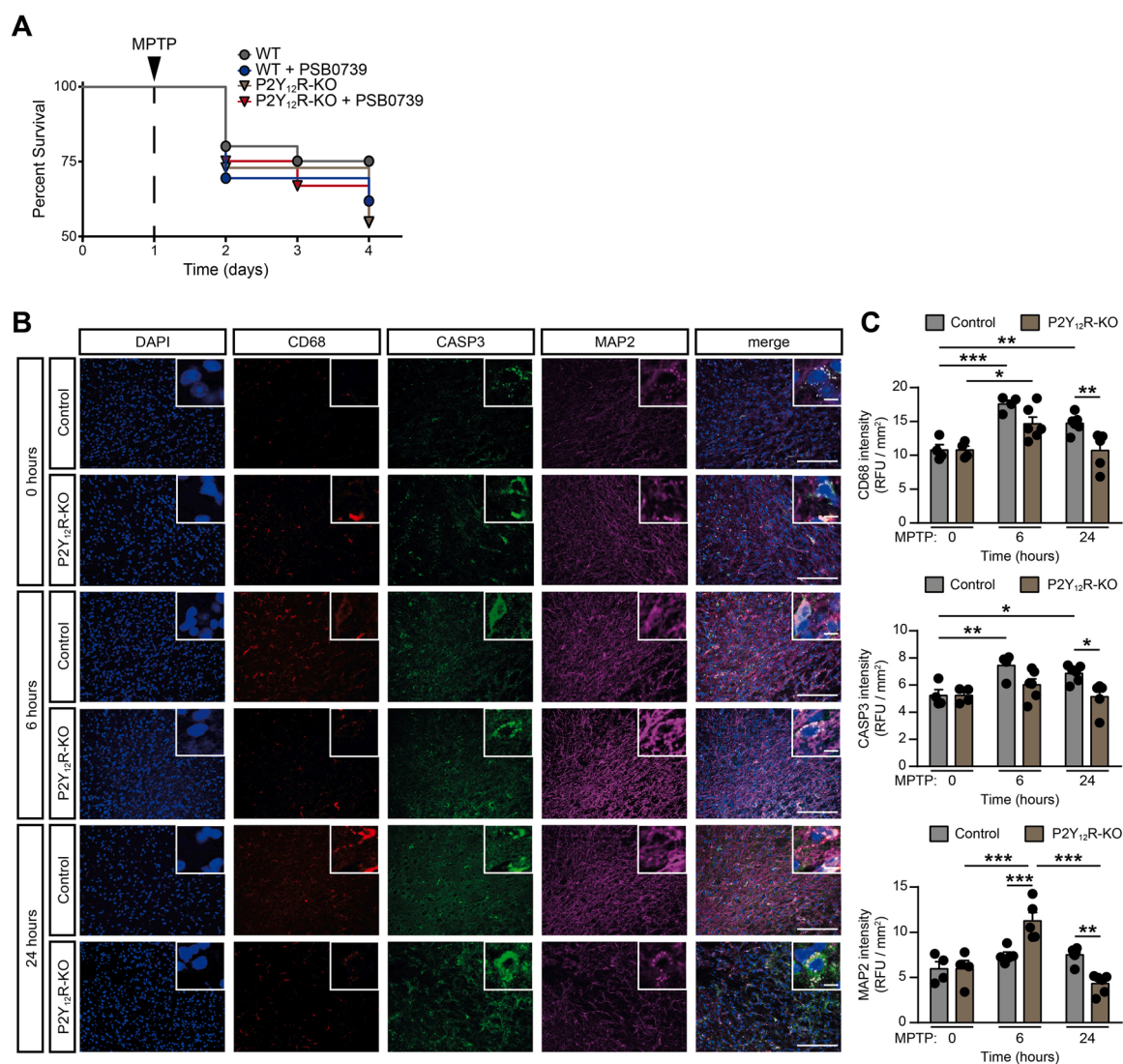

Fig. 1. P2Y$_{12}$-receptor invalidation promotes MPTP induced mortality and modulates the early phase of microglia activation **(A-C)** WT or P2Y$_{12}$-KO mice were pretreated with 0.3 mg / kg PSB 0739 or its vehicle and 4 × 20 mg / kg MPTP or its vehicle as indicated. Kaplan-Meier survival analysis performed on experimental groups receiving MPTP treatment (n = 21–24) (A). Representative immuno-confocal microscopy images of brain slices during the acute phase of MPTP administration isolated at the indicated time from WT or P2Y$_{12}$-KO mice, and stained with antibodies directed against CD68 (microsialin, red), Caspase-3 (CASP3, green), Microtubule-associated protein 2 (MAP2, purple), DAPI (blue) and overlay image (merge). Scale bar: 100 μm, corresponds to 20 μm inset (B) Quantification of CD68 fluorescence intensity (upper panel), CASP3 fluorescence intensity (middle panel) and MAP2 fluorescence intensity (lower panel) (n = 4–6, upper panel; n = 4–6, middle panel; n = 4–6, lower panel) (C). Data represent the mean ± SEM; * , $p \leq 0.05$; * *, $p \leq 0.01$; * ** , $p \leq 0.001$ (two-way ANOVA, with Bonferroni's *post-hoc* test (C)). (For interpretation of the references to colour in this figure legend, the reader is referred to the web version of this article.)

0739 group (*P = 0.0242* vs. *WT control*) and 45% in P2Y$_{12}$R-KO groups (*P = 0.0052* vs. *WT control*). This observation suggests that the presence of functional P2Y$_{12}$R is necessary to prevent the deterioration of acute neurotoxic events and to initiate disease resolution after MPTP treatment.

To further understand the acute effect of MPTP-administration and the role of dysfunctional P2Y$_{12}$R during early stages of the treatment, we have investigated microglia activation, cell apoptosis and neuron viability in wild-type control and P2Y$_{12}$R-KO mice before, at six hours and at twenty-four hours after the first MPTP injection. The myeloid specific lysosomal-associated membrane protein, CD68, was characterized as a microglial activation marker previously [38,39]; the cysteine-aspartic acid protease 3 (Caspase-3, CASP3) is a well described common apoptotic marker [40] and is activated by both extrinsic molecules (DAMPs) or intrinsic (mitochondrial) pathways [41]. The microtubule-associated protein 2 (MAP2) is known to be strongly and specifically expressed in the neuron perikarya and dendrites and its intensity can be used as an indirect marker of neuronal viability [42]. In our experiments, MPTP administration markedly increased CD68 and CASP3 fluorescence intensity in brain slices in the substantia nigra area both at six and twenty-four hours in wild-type control mice, compared to basal conditions (*P = 0.0001 and P = 0.0069 for CD68 and P = 0.0035 and P = 0.0168 for CASP3; respectively*), whereas MAP2 intensity was unchanged (*P = 0.6121 and P = 0.5354; respectively*) (Fig. 1B and C). These findings indicate prompt microglia activation and increased apoptosis in this early time period. In P2Y$_{12}$-receptor deficient animals, although MPTP-administration increased microglia activation at six hours compared to baseline conditions (*P = 0.008*), but not at twenty-four hours (*P = 0.9980*), and was significantly lower than in the wild-type control animals at this later point (*P = 0.0058* vs. *WT at 24 h*) (Fig. 1B and C). Likewise, Caspase-3 levels were lower, when compared to the wild-type control animals (*P = 0.0116* vs. *WT at 24 h*), and did not change significantly after MPTP-injection at six hours (*P = 0.2947*) and at twenty-four hours (*P = 0.9817*) compared to baseline conditions. MAP2 fluorescent intensity was markedly increased at six hours after MPTP-treatment in the P2Y$_{12}$R-KO animals (*P = 0.0001*), whereas it returned to the baseline level at twenty-four hours (*P = 0.1390*) (Fig. 1B and C). MAP2 intensity was significantly increased in the knock-out animals compared to the wild-type controls at six hours (*P = 0.0007* vs. *WT at 6 h*), and was significantly reduced at twenty-four hours (*P = 0.0018* vs. *WT at 24 h*) (Fig. 1C). These findings implicate that functional P2Y$_{12}$Rs are required following MPTP treatment for early, protective microglia activation, such as being able to phagocytose apoptotic cells, and thereby to prevent the spill over of intracellular contents, and further forestalling an uncontrolled neuroinflammatory state.

3.2. P2Y$_{12}$R gene deficiency and pharmacologic blockade is protective against MPTP-induced motor impairment, monoamine depletion, neurodegeneration and neuroinflammation

Next, we examined how genetic deletion or pharmacological blockade of P2Y$_{12}$R influences MPTP-induced neurodegeneration and motor function impairment. Administration of MPTP to wild-type mice resulted in severe motor function deterioration, when the latency to fall from rotarod apparatus was measured (*P = 0.0026 and P = 0.0034* vs. *WT control 6-hours and 24-hours post treatment, respectively*) (Fig. 2A). Surprisingly, inhibition of P2Y$_{12}$R, either genetically or with pharmacological blockade ameliorated motor function impairment in MPTP-treated mice (*P < 0.0001 and P = 0.039* vs. *MPTP-treated 6-hours post treatment, respectively*) (Fig. 2A). As expected, we found that administration of MPTP to wild-type mice induced selective degeneration of dopaminergic neurons in the substantia nigra *pars compacta* (Fig. 2B), demonstrated by reduced tyrosine-hydroxylase immunostaining and the presence of degenerating neurons with condensed nuclei, shrunken cytoplasm and prominent nuclear alterations (*P < 0.0001 WT control*

vs. *WT MPTP-treatment)*. MPTP-induced neurodegeneration was associated with reduced levels of monoamines, specifically dopamine (*P < 0.0001*), DOPAC (*P < 0.0001*), homovanillic acid (*P = 0.0174*) and noradrenaline (*P = 0.0005*) (Fig. 2C Supplementary Table 1) and decreased ATP levels in the striatum indicating a state of an energy deficit, as reflected by lower ATP/ADP ratio (*P = 0.0007*) (Supplementary Figure 2 A and B). Corroborating our findings on motor impairment, genetic deletion of the receptor protected from dopaminergic neuronal cell death in the substantia nigra *pars compacta* following MPTP-treatment (*P < 0.0012 WT MPTP-treatment* vs. *KO MPTP-treatment*) (Fig. 2B), mitigated the decrease in ATP concentration (*P = 0.7707*) and alleviated the reduction in MPTP-induced dopamine levels (*P < 0.0031 WT MPTP-treatment* vs. *KO MPTP-treatment)* in the striatum (Fig. 2C and Supplementary Figure 2 A). P2Y$_{12}$R gene deficiency had no effect on striatal noradrenaline (*P = 0.0887 WT MPTP-treatment* vs. *KO MPTP-treatment*), DOPAC (*P > 0.9999 WT MPTP-treatment* vs. *KO MPTP-treatment)* and homovanillic acid concentration (*P = 0.1005 WT MPTP-treatment* vs. *KO MPTP-treatment*) (Fig. 2C and Supplementary Fig. 2A).

Intrathecal administration of the selective P2Y$_{12}$-receptor antagonist PSB 0739 (0.3 mg/kg i.t.) 18 h prior to MPTP largely replicated the effect of P2Y$_{12}$R gene deficiency on MPTP-induced Parkinsonism in wild-type mice (Fig. 2D and E). In vehicle treated animals, MPTP administration promoted the degradation of dopaminergic neurons in the substantia nigra *pars compacta* (*P < 0.0001 WT control* vs. *WT MPTP-treatment*) (Fig. 2D), and reduced the concentration of monoamines, specifically dopamine (*P < 0.0001*), DOPAC (*P < 0.0001*), homovanillic acid (*P = 0.0270*) and noradrenaline (*P = 0.0004*) (Fig. 2E and Supplementary Table 1). PSB 0739 administration prevented the loss of TH-positive cells in the substantia nigra *pars compacta* (*P < 0.0001*) (Fig. 2D), and alleviated the depletion of dopamine (*P = 0.0031*), and noradrenaline levels in the striatum (Fig. 2E). Furthermore, pharmacological blockade of P2Y$_{12}$R with PSB 0739 in the P2Y$_{12}$R-KO mice had no further effect on monoamine concentration in the striatum following MPTP-treatment, when compared to vehicle treated littermate controls (*P = 0.2576 for dopamine; P = 0.9490 for noradrenaline; P > 0.9999 for DOPAC and P = 0.9035 for homovanillic acid*) (Fig. 2F). This finding indicates that PSB 0739 selectively act on P2Y$_{12}$R, and its effect requires the presence of functional receptors.

Additionally, we investigated the influence of PSB 0739 on MPTP-induced neuroinflammation and microglia activation. Treatment with MPTP in vehicle treated mice was also associated with neuroinflammation, characterized by increased levels of TNFα, IL-1β and IL-6 and the anti-inflammatory cytokine IL-10 in the striatum (*P = 0.0021; P < 0.0001; P = 0.0018 and P < 0.0001; respectively*) (Fig. 3B). PSB 0739 pre-treatment abolished the increase in cytokine levels in the substantia nigra (*P = 0.0004 for TNFα; P = 0.0005 for IL-1β; P = 0.0007 for IL-6 and P = 0.0688 for IL-10*) and the striatum (*P = 0.0004 for TNFα; P < 0.0001 for IL-1β; P = 0.0008 for IL-6 and P < 0.0001 for IL-10*) (Fig. 3A and B, respectively).

These data indicate that P2Y$_{12}$R in the central nervous system has a biphasic effect in the MPTP-induced Parkinson's disease model. Initially, functional P2Y$_{12}$R are essential to reduce the effects of acute toxicity; however, with the progression of the disease and the development of neuronal loss, P2Y$_{12}$R may further contribute to uncontrolled neuroinflammation. To further understand the mechanisms involved, we have also investigated the involvement of P2Y$_{12}$R in the modulation on dopamine release from the striatum. Although we could observe significant change in veratridine evoked [^{3}H]DA efflux in the slices of P2Y$_{12}$R-KO mice (*P = 0.0018*) indicating a potential neuromodulatory effect, this finding was not recapitulated by the P2Y$_{12}$-receptor antagonist PSB 0739 (no significant difference was observed) (Supplementary Figure 3).

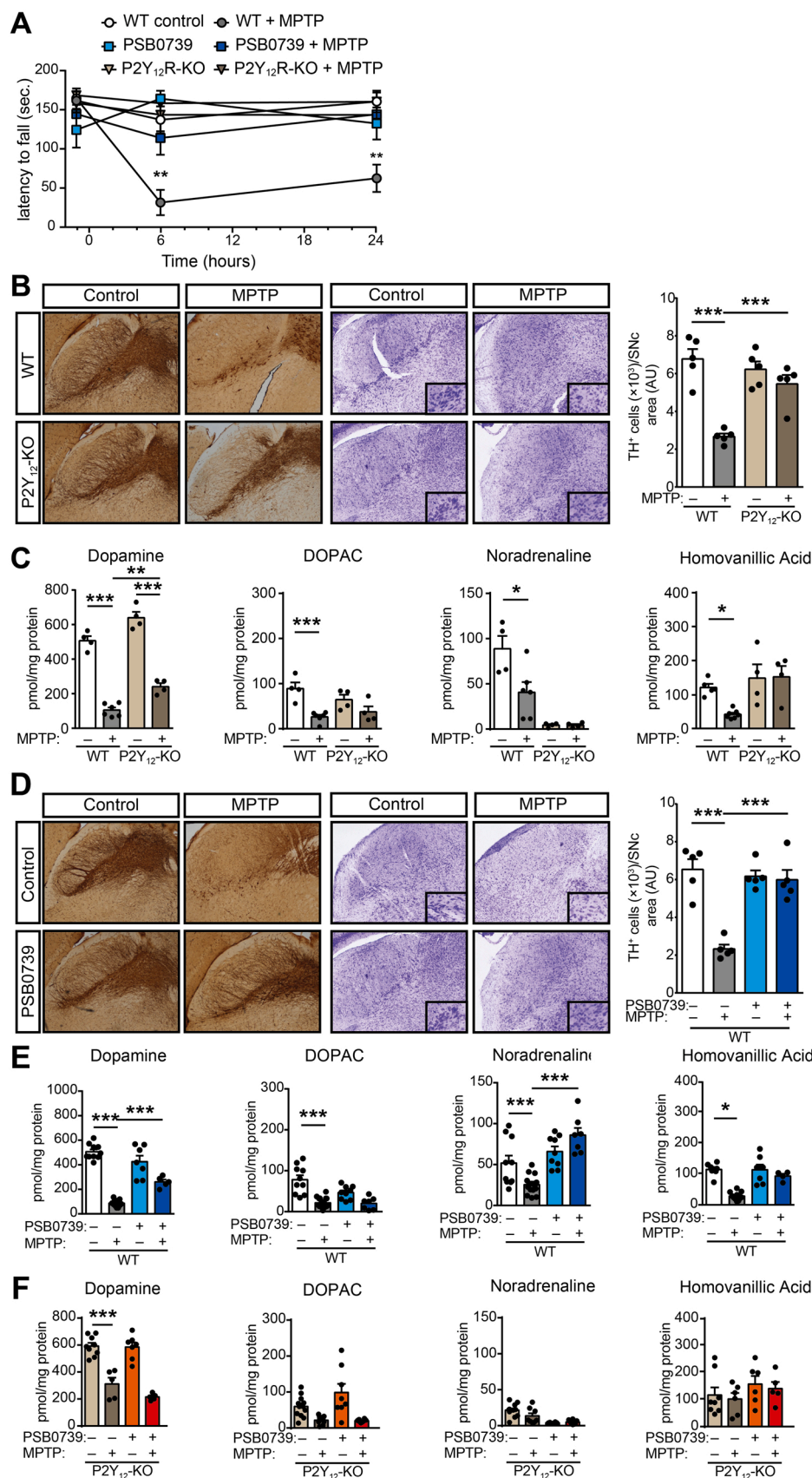**Fig. 2.** P2Y$_{12}$R gene deficiency and pharmacological blockade is protective against MPTP-induced motor impairment, monoamine depletion and neurodegeneration **(A-F)** WT or P2Y$_{12}$-KO mice were pretreated with 0.3 mg / kg PSB 0739 or its vehicle and 4 × 20 mg / kg MPTP or its vehicle as indicated. Effect of P2Y12R gene deficiency or 0.3 mg / kg PSB 0739 on the motor performance during MPTP induced PD measured on the rotarod test (n = 5–8) (A). Immuno-DAB staining for TH or cresyl violet staining on representative tissue sections after MPTP-treatment of WT or P2Y$_{12}$-KO mice; immunoreactivity is seen in the cell body and processes of dopaminergic and noradrenergic neurons (B); bar diagram shows the quantification of TH positive cells in the substantia nigra pars compacta (n = 5) (B, right panel). Concentration of dopamine, DOPAC, homovanillic acid and noradrenaline were determined from striatum samples of WT and P2Y12-KO mice 72 h after the initial MPTP administration (n = 4–6) (C). Immuno-DAB staining for TH or cresyl-violet staining on representative tissue sections after MPTP-treatment from PSB 0739 treated WT mice; immunoreactivity is seen in the cell body and processes of dopaminergic and noradrenergic neurons (D); bar diagram demonstrates the quantification of TH-positive cells in the substantia nigra pars compacta (n = 5) (D, right panel). Concentration of dopamine, DOPAC, homovanillic acid and noradrenaline were determined from striatum samples 72 h after the first MPTP administration (n = 5–15) (E); or from striatum samples of P2Y12-KO mice pretreated with PSB 0739 or its vehicle, 72 h after the initial MPTP injection (n = 5–12) (F). Data represent the mean ± SEM; *, $p \leq 0.05$; **, $p \leq 0.01$; ***, $p \leq 0.001$ (two-way ANOVA, with Tukey's *post-hoc* test (A-F)).
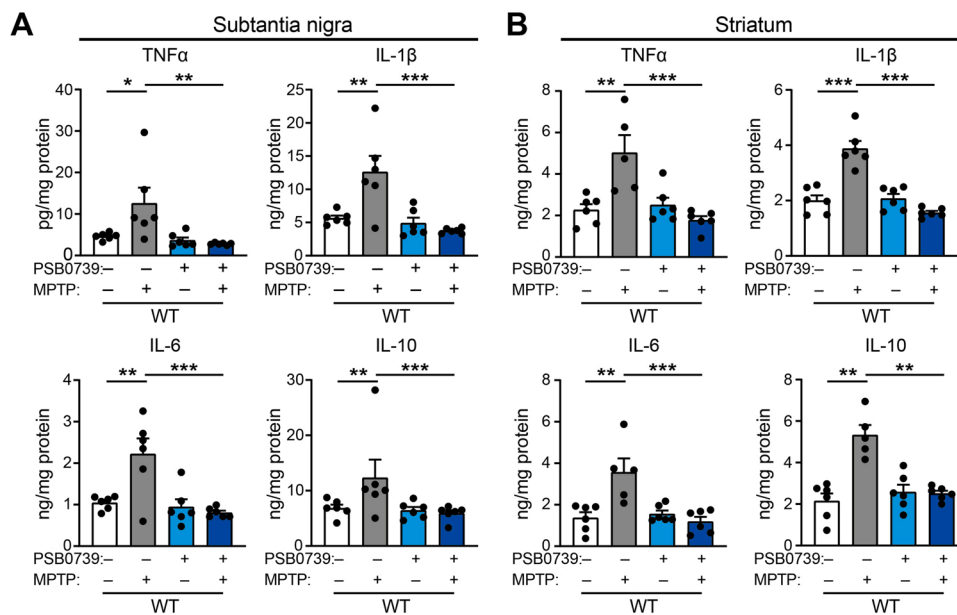
Fig. 3. Pharmacological blockade of P2Y$_{12}$R abrogates MPTP-induced pro-inflammatory cytokine production in the striatum **(A-B)** WT mice were pretreated with 0.3 mg / kg PSB 0739 or its vehicle and 4 × 20 mg / kg MPTP or its vehicle as indicated. TNFα, IL-1β, IL-6 and IL-10 concentration measured from substantia nigra (n = 5) (A) or striatum samples (n = 5) (B). Data represent the mean ± SEM; *, $p \leq 0.05$; * *, $p \leq 0.01$; *** , $p \leq 0.001$ (two-way ANOVA, with Bonferroni's *post-hoc* test (A-B)).

3.3. P2Y$_{12}$-receptor blockade halts disease progression after subchronic MPTP administration

Since our data implicated a pivotal role for P2Y$_{12}$R in neuro-inflammation, we further investigated the contribution of P2Y$_{12}$R using an animal model of MPTP-induced subchronic neurodegeneration. To account for the markedly different survival rate of wild-type and P2Y$_{12}$R deficient animals during the acute experimental PD model, an alternative MPTP treatment protocol was used to explore P2Y$_{12}$R actions during disease progression; rather than administering the P2Y$_{12}$R-inhibitor prior to MPTP, a subchronic Parkinson's disease model was generated by a single daily administration of MPTP over the course of five days, followed by receptor blockade for four consecutive days (Supplementary Figure 1B). During the early phase of the MPTP treatment, on day five to six, limited effect could be observed on dopaminergic neuron loss in wild-type and P2Y$_{12}$R-KO mice ($P = 0.0576$ and $P = 0.6108$; respectively) (Fig. 4A). However, twenty-one days following MPTP administration, we detected significant loss of dopaminergic neurons in the substantia nigra *pars compacta* ($P < 0.0001$) (Fig. 4B), reduction in dopamine, DOPAC, noradrenaline and homovanillic acid levels ($P < 0.0001$; $P = 0.0082$; $P = 0.0095$ and $P < 0.0001$; respectively) (Fig. 4C), and markedly decreased motor functions ($P = 0.0206$) (Fig. 4D). P2Y$_{12}$R inhibition increased dopaminergic cell survival ($P < 0.0001$) (Fig. 4B), reduced the decrease in dopamine, noradrenaline and homovanillic acid levels ($P = 0.0002$; $P = 0.0039$ and $P = 0.0057$; respectively) (Fig. 4C), and prevented deterioration in motor function ($P = 0.9950$) (Fig. 4D) assessed three weeks after treatment. Furthermore, using this model, there was no difference in the survival rate between the experimental groups (Fig. 4E).

3.4. P2Y$_{12}$-receptor mediates microglia activation via Rho-kinase and p38 MAPK phosphorylation

To characterize the intracellular mechanism underlying the protective effect of P2Y$_{12}$R blockade, the relationship between P2Y$_{12}$R stimulation and microglia activation was investigated. Initially, since the activation of p38 mitogen-activated protein kinase (p38 MAPK) can directly promote or indirectly stimulate cytokine production via MK2 or MSK1/2 in microglia [43–46], changes in the p38 MAPK activity was measured. Phosphorylation of p38 MAPK at Threonine 180 / Tyrosine 182 increases the kinase activity, thus promoting phosphorylation of

several transcriptional factors and further bolster inflammatory cytokine biosynthesis [47]. In initial experiments we confirmed that treatment with LPS (1 μg / ml, 60 min) or the P2Y$_{12}$R agonist ADP (10 μM, 60 min) promotes p38 MAPK phosphorylation at T 180 / Y 182 in vitro ($P = 0.0002$ and $P < 0.0001$; respectively) (Fig. 5A and B) using murine microglial cell line BV-2. The small GTPase, Ras homolog family member A (RhoA) and the downstream effector, Rho-associated, coiled-coil containing protein kinase 1 (ROCK1) has been previously shown to mediate p38 MAPK phosphorylation and activation [48]; we have tested the effect of the ROCK1 inhibitor, Y-27632, on LPS or ADP-induced p38 MAPK activation. Pretreatment with Y-27632 (10 μM, 30 min) markedly decreased LPS or ADP-induced p38 MAPK phosphorylation ($P = 0.0044$ and $P = 0.0013$; respectively) (Fig. 5B); additionally, pretreatment with the selective P2Y$_{12}$R inhibitor, PSB 0739 (500 nM, 30 min) blocked ADP-induced, but not LPS-induced p38 MAPK activation ($P = 0.0007$ and $P = 0.9999$; respectively) (Fig. 5A). These results indicate that under in vitro conditions, both P2Y$_{12}$R and ROCK1 are necessary for ADP-mediated p38 MAPK phosphorylation. To confirm the influence of P2Y$_{12}$R on p38 MAPK phosphorylation and microglia activation, as well as on the cytokine levels produced by microglia in vitro, murine microglia cells were treated with the ectonucleotidase inhibitor ARL 67156 (30 μM, 20 min) combined with either PSB 0739 (500 nM, 20 min) or with the solvent [49]. Cells were stimulated with ADP (100 μM) for six or twenty-four hours, and microglia activation and p38 MAPK phosphorylation at Threonine 180 / Tyrosine 182 were analysed (Fig. 5C and D). ADP stimulation markedly increased CD68 fluorescence intensity at six and at twenty-four hours compared to basal conditions ($P = 0.0005$ and $P < 0.0001$ at 6 and 24 h; respectively), whereas phosphorylated p38 MAPK intensity was unchanged at six hours ($P = 0.4343$), but was significantly increased at twenty-four hours ($P < 0.0001$) (Fig. 5C and D). In cells treated with P2Y$_{12}$-receptor antagonist, ADP administration was without effect on microglia activation and p38 MAPK phosphorylation compared to the baseline condition ($P = 0.3342$ and $P = 0.9994$ at 6 and 24 h for CD68; and $P = 0.7589$ and $P = 0.3572$ at 6 and 24 h for p-p38 MAPK; respectively), and was significantly different from the control cells ($P = 0.0138$ and $P < 0.0001$ vs. *Control* at 6 and 24 h for CD68; and $P < 0.0001$ vs. *Control* at 24 h for p-p38 MAPK; respectively) (Fig. 5C and D). Stimulation with ADP was also associated with increased production of TNFα ($P = 0.0191$ and $P < 0.0001$ at 6 and 24 h; respectively), IL-1β at twenty-four hours ($P = 0.2340$ and $P < 0.0001$ at 6 and 24 h;
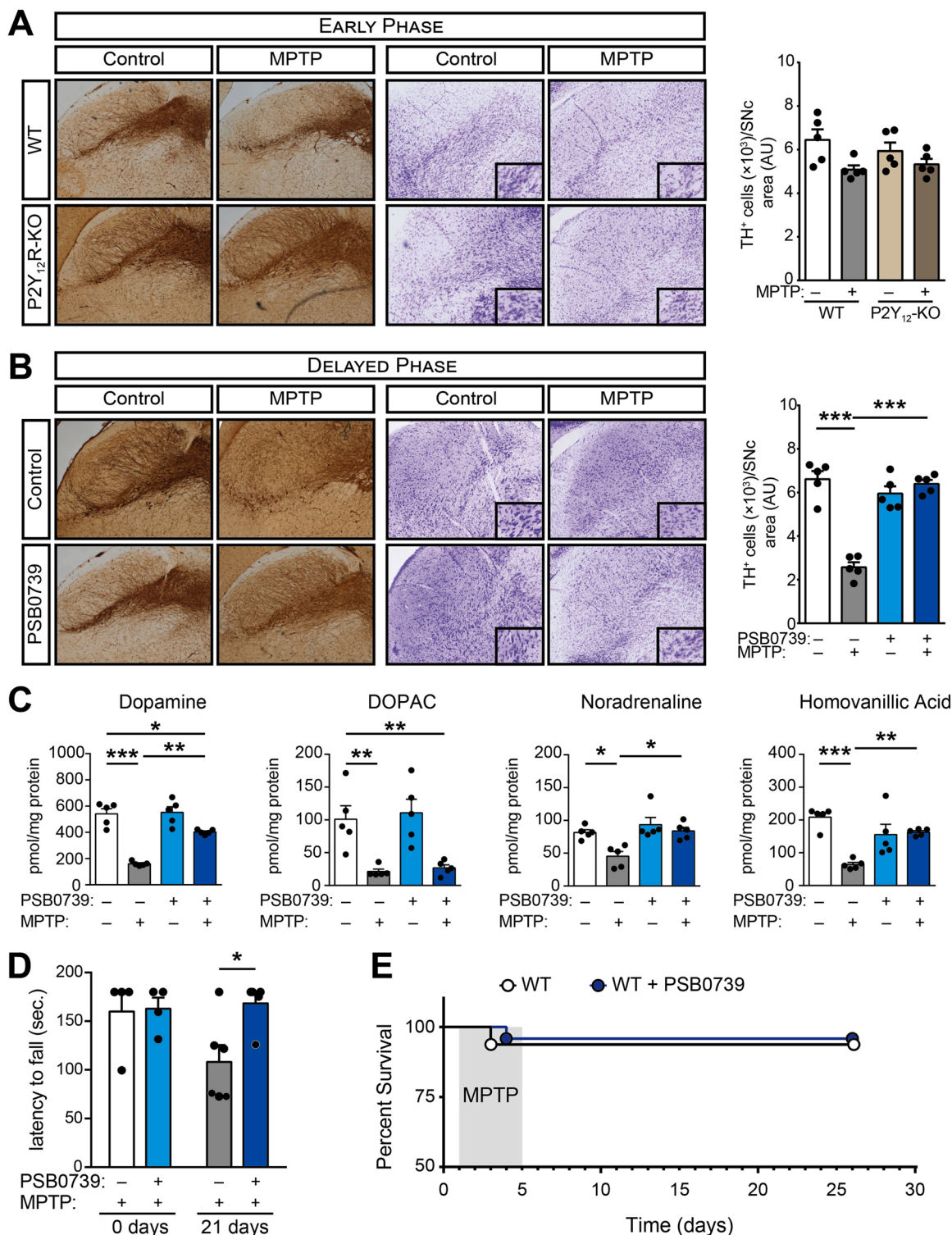
Fig. 4. P2Y$_{12}$R blockade halts disease progression **(A-E)** WT or P2Y$_{12}$-KO mice were treated with 20 mg / kg MPTP daily for five consecutive days, followed by treatment with 0.3 mg / kg PSB 0739 or its vehicle. Immuno-DAB staining for TH and cresyl-violet staining on representative tissue sections five days after the initial MPTP administration; immunoreactivity is seen in the cell body and processes of dopaminergic and noradrenergic neurons (A); bar diagram shows the quantification of TH-positive cells in the substantia nigra *pars compacta* (n = 5) (A, right panel). Immuno-DAB staining for TH and cresyl-violet staining on representative tissue sections 21 days after the last PSB 0739 treatment (B); bar diagram displays the quantification of TH-positive cells in the substantia nigra pars compacta (n = 5) (B, right panel). Concentration of dopamine, DOPAC, homovanillic acid and noradrenaline were determined from striatum samples 21 days after last PSB 0739 administration (n = 5) (C). Effect of PSB 0739 or its vehicle on the motor performance during MPTP-induced PD measured on the rotarod test before and 21 days after treatment (n = 4–6) (D). Kaplan-Meier survival analysis performed on experimental groups receiving MPTP treatment (n = 8–16) (E). Data represent the mean ± SEM; *, $p \leq 0.05$; **, $p \leq 0.01$; ***, $p \leq 0.001$ (two-way ANOVA, with Bonferroni's *post-hoc* test (A-D)).
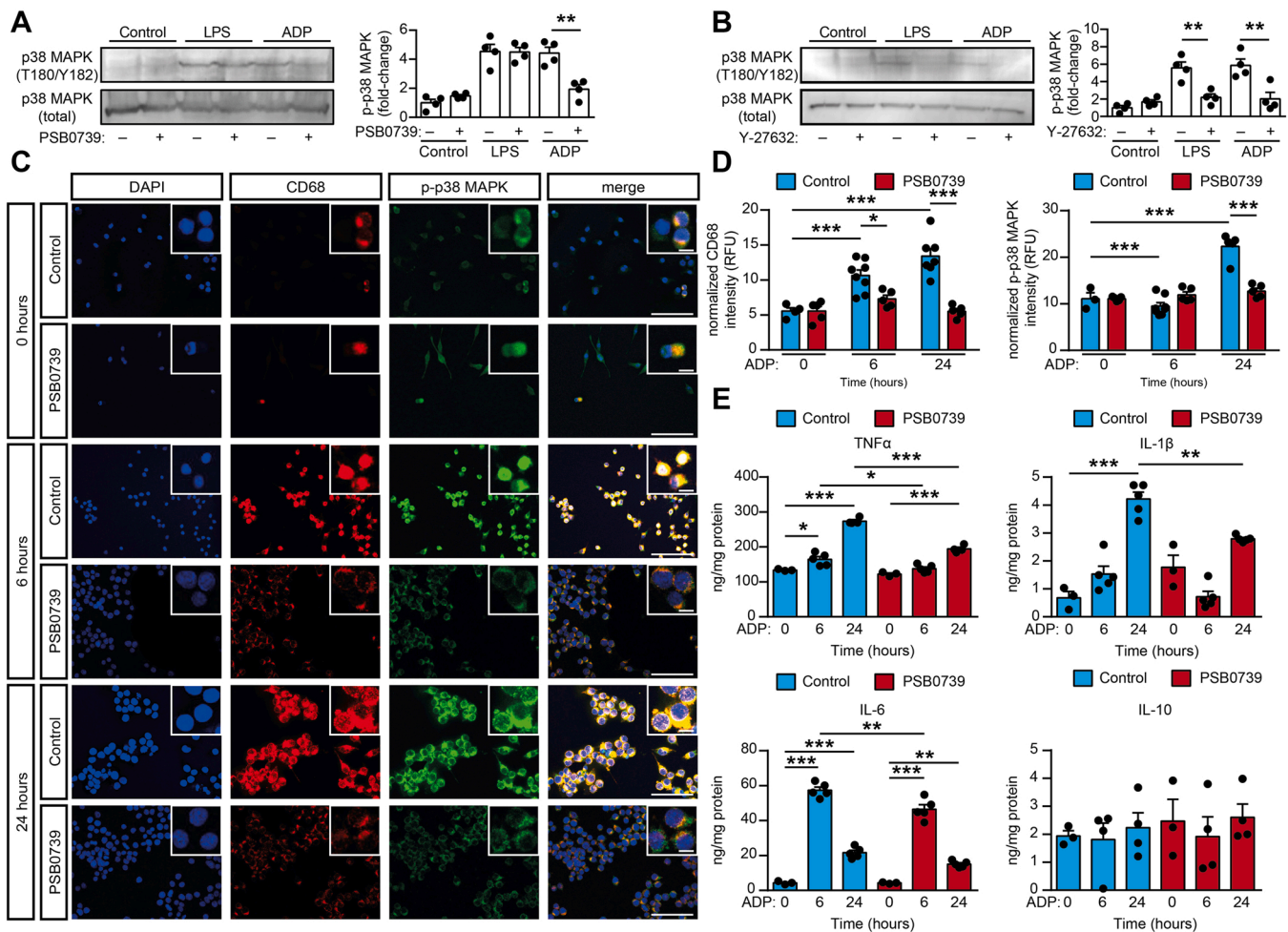
Fig. 5. P2Y$_{12}$R mediates ADP-induced microglia activation in vitro to control cytokine production via Rho-kinase-dependent p38 MAPK phosphorylation **(A-B)** Murine BV-2 microglia cells were pretreated with PSB 0739 (500 nM, 30 min) (A) or with Y-27632 (10 μM, 30 min) (B) and were incubated with LPS (100 ng / ml, 60 min), ADP (10 μM, 5 min) or solvent (control) and phosphorylation of p38 MAPK at Threonine 180 / Tyrosine 182 were determined by immunoblotting. Graphs show the densitometric evaluation (n = 4). **(C-E)** Murine BV-2 microglia cells were pretreated with ARL 67156 (30 μM, 20 min) combined with PSB 0739 (500 nM, 30 min) or the solvent (Control) as indicated; thereafter, ADP (100 μM) was added to the extracellular solution for the indicated time periods to induce microglia activation and cytokine production. Shown are representative immuno-confocal microscopy images of cultured cells after ADP administration, and stained with antibodies directed against CD68 (microsialin, red), phosphorylated-p38 MAPK (green), DAPI (blue) and overlay image (merge). Scale bar: 100 μm, corresponds to 20 μm inset (C) Quantification of CD68 fluorescence intensity (left panel), and phosphorylated-p38 MAPK fluorescence intensity (right panel) (n = 4–8, left panel; n = 3–7, right panel). Values were normalized to the average fluorescent intensity of Iba1 staining (not shown) (D). TNFα, IL-1β, IL-6 and IL-10 concentration measured from the cultured cell supernatant at 0, 6 and 24 h of ADP stimulation (n = 3–5) (E). Data represent the mean ± SEM; *, $p \leq 0.05$; **, $p \leq 0.01$; ***, $p \leq 0.001$ (two-way ANOVA with Bonferroni's *post-hoc* test (A, B, D, E)). (For interpretation of the references to colour in this figure legend, the reader is referred to the web version of this article.)

respectively) and IL-6 ($P < 0.0001$ and $P < 0.0001$ at 6 and 24 h; respectively) but not the anti-inflammatory cytokine IL-10 (concentration of IL-10 was below the detection limit) (Fig. 5E). P2Y$_{12}$-receptor blockade reduced TNFα ($P = 0.0179$ and $P < 0.0001$ vs. *Control* at 6 and 24 h; respectively), IL-1β at twenty-four hours ($P = 0.1547$ and $P = 0.0027$ vs. *Control* at 6 and 24 h; respectively) and IL-6 levels at six hours ($P = 0.0013$ and $P = 0.0866$ vs. *Control* at 6 and 24 h; respectively) (Fig. 5E).

Next, the involvement of P2Y$_{12}$R and ROCK1 blockade on p38 MAPK phosphorylation and microglia activation under in vivo conditions was tested. Apart from the myeloid specific lysosomal-associated membrane protein (CD68); the ionized calcium-binding adapter molecule 1 (Iba1), which is known to be strongly and specifically expressed in both senescent and activated microglia [50] was stained. In our experiments, MPTP administration markedly increased phospho-p38 MAPK T180/Y182 and CD68 fluorescence intensity in brain slices in the substantia nigra area compared to saline treated control animals ($P = 0.0063$ and $P = 0.0003$; respectively), whereas Iba1 intensity was

unchanged ($P = 0.9931$) 21 days after treatment (Fig. 6A and B). Intrathecal administration of 0.3 mg / kg PSB 0739 alone was without effect. However, P2Y$_{12}$-receptor blockade significantly reduced MPTP-induced p38 MAPK activity and microglia activation, measured by phospho-p38 MAPK T180/Y182 and CD68 positivity ($P = 0.0406$ and $P = 0.0026$; respectively) (Fig. 6A and B). To assess ROCK1 involvement, the specific ROCK1 inhibitor fasudil, which has the advantage over Y-27632 that it does not require parenteral administration, was orally delivered in the drinking water (50 mg / kg body weight per day) [27] (Supplementary Figure 1 C). Fasudil-treatment alone had no effect on phospho-p38 MAPK T180/Y182 or CD68 fluorescence intensity. When fasudil was administered during MPTP-treatment, CD68 and phosphorylated-p38 MAPK fluorescence intensity was significantly reduced in comparison to MPTP-treatment alone ($P = 0.0181$ and $P = 0.0034$; respectively) (Fig. 6A and B). No changes could be observed in both p38 MAPK and Iba1 fluorescence intensity between control, MPTP treated or MPTP combined with PSB 0739 or fasudil-treated groups ($P = 0.1621$; $P = 0.1371$ and $P = 0.6200$ for p38 MAPK; and
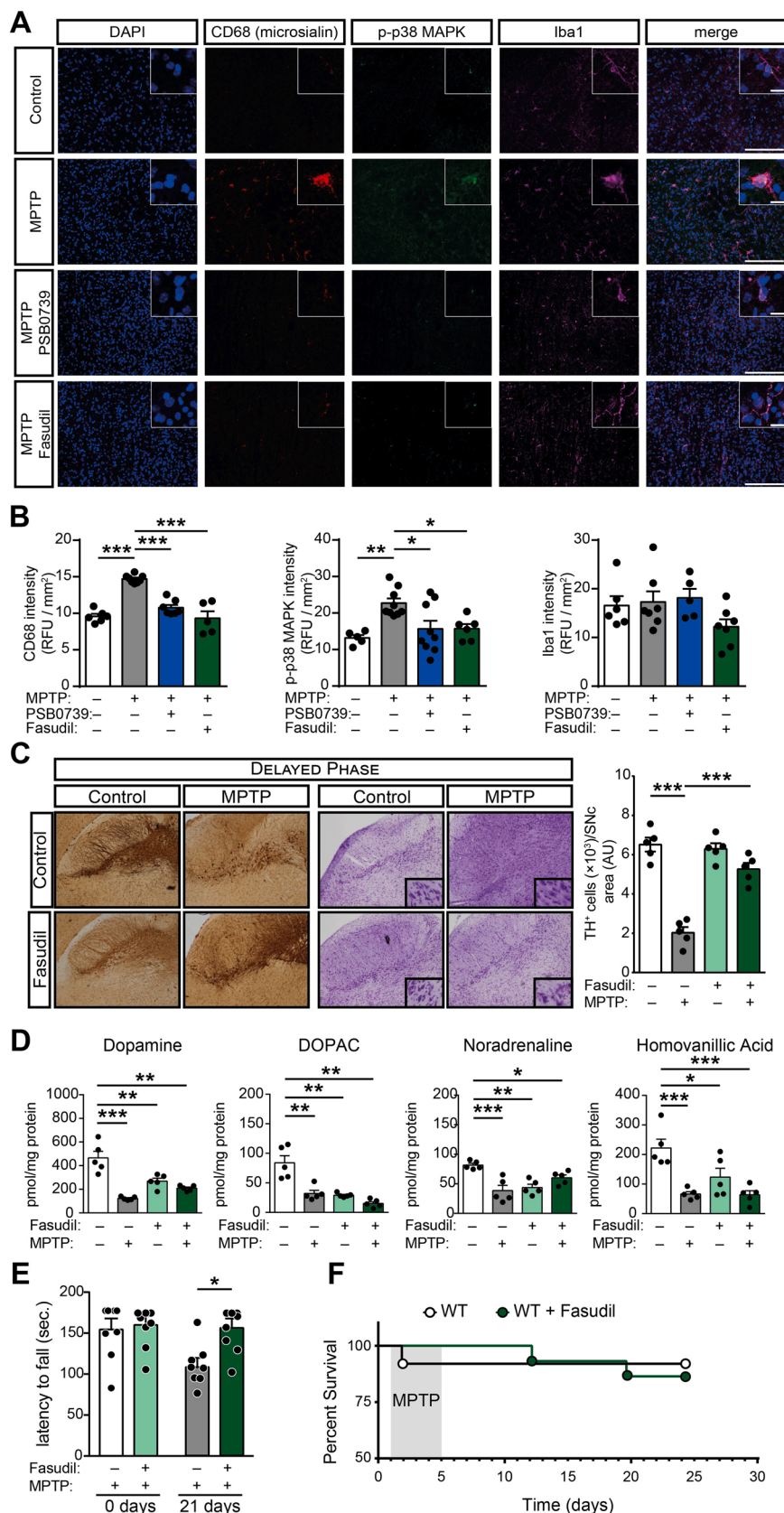
Fig. 6. Pharmacological P2Y$_{12}$R or Rho-kinase blockade in vivo abolish microglia activation, interrupts disease progression and alleviates MPTP-induced Parkinsonism **(A-F)** WT mice were treated with 20 mg / kg MPTP daily for five consecutive days, followed by treatment with 0.3 mg / kg PSB 0739, 50 mg / kg body weight per day fasudil or its vehicle. Shown are representative immuno-confocal microscopy images of brain slices isolated from WT mice stained with antibodies directed against CD68 (microsialin, red), phosphorylated-p38 MAPK (green), Iba1 (purple), DAPI (blue) and overlay image (merge). Scale bar: 100 μm, corresponds to 20 μm inset (A) Quantification of CD68 fluorescence intensity (left panel), phosphorylated-p38 MAPK fluorescence intensity (middle panel) and Iba1 fluorescence intensity (right panel) (n = 5–8, left panel; n = 5–9, middle panel; n = 5–7, right panel) (B). Representative images of immuno-DAB staining for TH and cresyl-violet staining on tissue sections 21 days after the last treatment; immunoreactivity is seen in the cell body and processes of dopaminergic and noradrenergic neurons (C); bar diagram show quantification of TH-positive cells in the substantia nigra pars compacta (n = 5) (C, right panel). Concentration of dopamine, DOPAC, homovanillic acid and noradrenaline were determined from striatum samples 21 days after last treatment (n = 5) (D). Effect of fasudil or its vehicle on the motor performance during MPTP-induced PD measured on the rotarod test before and 21 days after treatment (n = 8) (E). Kaplan-Meier survival analysis performed on experimental groups receiving MPTP treatment (n = 8–10) (F). Data represent the mean ± SEM; *, $p \leq 0.05$; **, $p \leq 0.01$; ***, $p \leq 0.001$ (two-way ANOVA, with Bonferroni's *post-hoc* test (B-E)). (For interpretation of the references to colour in this figure legend, the reader is referred to the web version of this article.)

$P = 0.2457; P = 0.6875$ and $P = 0.9995$ for Iba1; respectively) (Supplementary Figure 4 A and B).

Since our data strongly suggest ROCK1 to be also involved in MPTP-induced neuroinflammation, we further investigated the involvement of ROCK1 during neurodegeneration. Similar to our previously shown results utilizing the subchronic Parkinson's disease model, MPTP administration induced significant loss of dopaminergic neurons in the substantia nigra *pars compacta* ($P < 0.0001$) (Fig. 6C), reduction in dopamine, DOPAC, noradrenaline and homovanillic acid levels ($P < 0.0001; P = 0.0003; P = 0.0006$ and $P = 0.0009$; respectively) (Fig. 6D), and markedly decreased motor functions ($P = 0.0460$) 21 days after the last MPTP dose (Fig. 6E). Fasudil-treatment increased dopaminergic cell survival ($P < 0.0001$) (Fig. 6C) and improved motor function ($P = 0.0373$) (Fig. 6E). Interestingly, treatment with fasudil only (without MPTP administration) substantially reduced monoamine levels in the striatum ($P = 0.0021$ for dopamine; $P = 0.0002$ for DOPAC; $P = 0.0019$ for noradrenaline and $P = 0.0327$ for homovanillic acid) (Fig. 6D). When fasudil-treatment was combined with subchronic MPTP administration, the decrease in dopamine concentration in the striatum was alleviated compared to the MPTP-induced decrease ($P = 0.5400$) (Fig. 6D). Furthermore, we could not find difference in the survival rate in response to fasudil administration in MPTP treated mice (Fig. 6F).

Lastly, we have examined P2Y$_{12}$R immunostaining in the substantia nigra in the MPTP-induced animal model and in post-mortem samples derived from Parkinson's disease patients. The specificity of the P2Y$_{12}$R antibody has been validated using wild-type control and P2Y$_{12}$R-KO mice (Supplementary Fig. 5A and B). P2Y$_{12}$R immunoreactivity displayed co-localization with CD68 in the substantia nigra verifying its association with the activated microglia in this particular brain area relevant for Parkinson's disease. No changes could be observed in P2Y$_{12}$R fluorescence intensity between control, MPTP-treated or MPTP combined with PSB 0739 or Fasudil-treated groups (Supplementary Fig. 5C). P2Y$_{12}$R expression is also demonstrated on cells with typical morphology of activated microglial cells in the neocortex (Supplementary Fig. 5D, left and middle panel) and striatum (Supplementary Figure 5D, right panel) of patients with Parkinson's disease dementia (i. e. Parkinson's disease patients who developed dementia at the late stage of the disease).

4. Discussion

Here we report for the first time the involvement of the purinergic P2Y$_{12}$-receptors in experimental Parkinsonism in mice. Our most intriguing, principal finding is that P2Y$_{12}$R have a dualistic role in the MPTP-induced Parkinson's disease model. Pharmacological inhibitors of P2Y$_{12}$R are widely used in clinical practice to inhibit platelet aggregation and thereby prevent stroke and myocardial infarction [51]. Single cell RNA sequencing [52] and molecular biology experiments [53], as well as our data demonstrates that in the rodent and human CNS, P2Y$_{12}$R are preferentially expressed on microglia [54]; therefore it is reasonable to assume that the primary target for intrathecally administered PSB 0739 are microglia. Interestingly, since it has been shown that microglia and astrocytes (or even oligodendrocytes [55]) interact extensively to form specialized nanoarchitecture [10], the modified activity of P2Y12Rs expressed on microglia can still influence astrocytic cell function to induce the release of neurotrophic factors. However, this interaction and the role of purinergic receptors in regulating astrocytic cell function would require further investigation.

Since P2Y$_{12}$R-KO and PSB 0739-treated mice displayed similar effects on disease progression, our results suggest that while the presence of P2Y$_{12}$R is essential to prevent acute neurotoxicity and associated mortality; prolonged activation of P2Y$_{12}$R may alter pro- and anti-inflammatory cytokine production, maintain neuroinflammation and contribute to the progressive neurodegeneration of the nigrostriatal dopaminergic pathway during experimental Parkinsonism. Under physiological circumstances, microglia perform constant surveillance of the brain parenchyma. They exhibit ramified morphology, where long cytoplasmic processes survey their surrounding environment [56]. Exogenous stimuli, such as bacterial endotoxin lipopolysaccharide, IFNγ, trauma, reperfusion-injury or chemical toxins induce microglial activation [57] to stimulate the activity of iNOS, modulate the expression of various cell surface markers (i.e. CD68, CD11b, MHC-II), and to increase pro-inflammatory cytokine (IL-1β, IL-6 and TNFα) and chemokine (CCL2, CXCL10) production [58]. On the other hand, microglia is indispensable for the resolution of inflammation, where microglia produces anti-inflammatory mediators, such as IL-4, IL-10, extracellular matrix proteins or glucocorticoids [59]. Neuroinflammation has a central role in Parkinson's disease pathogenesis [12]; characterized by microglial proliferation, activation and production of inflammatory mediators [59,60]. While microglia seemingly maintain neuroinflammation and exacerbate Parkinson's disease symptoms, the presence of functional microglia also appears to be essential to reduce neurotoxic effects, which issue has been highly controversial in PD and in other forms of neurodegeneration [61]. For example, it has been shown that microglia depletion via the CSF1R inhibitor PLX3397, aggravates the impairment in locomotor activity, worsens the loss of dopaminergic neurons and augments the infiltration of leukocytes into the brain after MPTP treatment [62]. Here we provide novel insights into the mechanisms of experimental PD to resolve some of the controversies presented above. During the early stages following a neurotoxic event, affected cells exhibit a wide range of the cell death spectrum, where the classical apoptosis and necrosis are assumed to be the two extremes of the spectrum [63]. We have found that Caspase-3 levels are rapidly increased after MPTP-administration in wild-type control, but not in P2Y$_{12}$R-KO mice, implying the role of this receptor in the initiation of programmed, apoptotic cell death; moreover, the neuronal viability marker MAP2 was markedly reduced in the gene-deficient animals at 24 h, suggesting a shift towards necrotic cellular death. These findings indicate that during pathophysiological conditions, the regulated and appropriate activation of microglia is necessary to shift the cell death spectrum towards the anti-inflammatory apoptosis (and potentially necroptosis) to avoid the rapid lysis of cells and the release of cellular constituents including damage-associated molecular patterns (DAMPs), thus preventing the exacerbation of inflammation. Moreover, P2Y$_{12}$R appear to be central regulators for sensing DAMPs and initiating and facilitating phagocytosis of necrotic cells [64,65], thereby halting the aggravation of inflammation. Recently, we revealed the pivotal role for P2Y$_{12}$R during microglia-neuron communication through somatic purinergic junctions [10]; where the interaction sites between the neuronal cell bodies and microglial processes create a highly specialized nanoarchitecture through which microglia monitor neuronal activity and mediate neuroprotection via P2Y$_{12}$R upon acute brain injury. These interactions may explain the early protective actions by microglial P2Y$_{12}$R to prevent mortality after MPTP administration, while these sites may also function as initiators for microglial phagocytosis around terminally injured neurons [10]. Nevertheless, the role of other P2Y$_{12}$R-driven actions, interacting with the robust, systemic toxicity of MPTP cannot be entirely excluded in case of the acute MPTP protocol.

Contrarily, chronic inhibition of P2Y$_{12}$R during disease progression mitigates inflammation, protects against dopaminergic neuronal cell loss and alleviates motor impairments. Previous work has already indicated the role of P2Y$_{12}$ purinergic receptors in both the maintenance of neuroinflammation and facilitation of tissue repair [66]. For instance, P2Y$_{12}$R modulate microglial activation, migration and polarization via phosphoinositde-3-kinase (PI3K) activation and AKT phosphorylation [11,67]. We have previously showed that P2Y$_{12}$R regulate hyperalgesia and local inflammatory processes, and also contribute to the development of chronic hindpaw inflammation [9]; while P2Y$_{12}$R located on microglia affect neuropathic pain via GTP-RhoA/ROCK pathway and p38 MAPK activation after spinal cord injury [68]. However the contribution of P2Y$_{12}$R to neurodegeneration in PD has not been

explored until now. As for the molecular mechanisms that link $P2Y_{12}$ signalling with cytokine production in the present experimental model, we propose that DAMPs bind to $P2Y_{12}R$, which via the $G\alpha_i$ subunit reduces the intracellular cAMP concentration. The consequential decrease in protein kinase A activity results in increased RhoA activity, presumably due to the decreased phosphorylation state of the inhibitory Serine 188 site on RhoA, leading to increased ROCK activity [48]. Enhanced ROCK activity further promotes Threonine 180 / Tyrosine 182 phosphorylation on p38 MAPK, whereas the simultaneous double phosphorylation on p38 MAPK stimulates the kinase activity inducing the transcription and production of cytokines [69] (Fig. 7). Interestingly, aside from ROCK-mediated activation of p38 MAPK, the MAPK pathway can also be activated by cytokines, namely IL-1β and TNFα [70,71]; providing an enhancing feed-back loop to inflammation. This can lead to a circumstance, where a specific stimulus activating p38 MAPK promotes inflammation and cytokine production, and enters into a vicious cycle, where inflammation maintains inflammation. However, if this cycle could be selectively disrupted, disease resolution would be an advantageous outcome.

Apparently, at the onset of neuroinflammation, microglial phagocytosis might serve as an essential prerequisite for ceasing the exacerbation of inflammation and cell death [64], while creating a favorable environment for neuronal survival. Scheiblich et al. found that RhoA inhibition decreased microglial phagocytosis of neuronal cell fragments, while blockade of the downstream effector ROCK with Y-27632 or Fasudil reduced the engulfment of neuronal debris and attenuated the production of inflammatory mediators [72]. These findings indicate that activation of the RhoA / ROCK pathway during the neuroprotective phase of the event is central for the initiation of phagocytosis and clearance of cellular debris; however, the same pathway is responsible for maintaining the disproportionate and lasting activation of microglia, which may govern widespread neurodegeneration. The most likely possibility is that this switch occurs gradually. Based on our data the we can roughly estimate the time course of the neuroinflammatory events, and we have found that the switch between neuroprotective and neurodegenerative effect occurs between the fifth day and day twenty-one of the subchronic treatment protocol. During the early phase, neurodegeneration was limited in the MPTP-treated mice, while at the delayed phase, neurodegeneration was prominent in the wild-type MPTP-treated, but not in the P2Y12R-deficient group. Additionally, coupled to the increased neuronal cell death and high-number of activated microglia, sustained ROCK activation was present in the wild-type animals during the delayed phase of neuroinflammation, since ROCK inhibition by Fasudil prevented neurodegeneration and microglia activation.

Recently, the potentially advantageous effect of Rho-kinase inhibition in several neurodegenerative disorders has been demonstrated [8, 73]. Fasudil-administration proved to inhibit axonal degeneration and neuronal death in an experimental Parkinson's disease model, when administered prior to disease onset [63,74]. Furthermore, ROCK inhibitors were postulated to promote the activity of Parkin-mediated mitophagy pathway during PD, by recruiting HK2, a positive regulator of Parkin, to mitochondria. The increased Parkin recruitment to damaged mitochondria leads to increased removal of mitochondria from injured cells [8]. However, a side effect of Rho-kinase inhibition, namely the stimulation of monoamine oxidase activity, was previously demonstrated [75]. Since increased monoamine oxidase activity leads to rapid metabolism of monoamines, this crucial observation may also explain our finding that prolonged fasudil-treatment lead to the reduction in central monoamine levels, and proposes a potential limitation on the application of fasudil in the treatment of Parkinson's disease. Our data indicate that modulating P2Y12R activity has a highly specific protective influence in MPTP-induced Parkinsonism, without the observed adverse effects of fasudil; consequently P2Y12R-inhibition might be more advantageous in the treatment of Parkinson's disease. Finally, the human relevance of our work is underscored by the recent work performed by
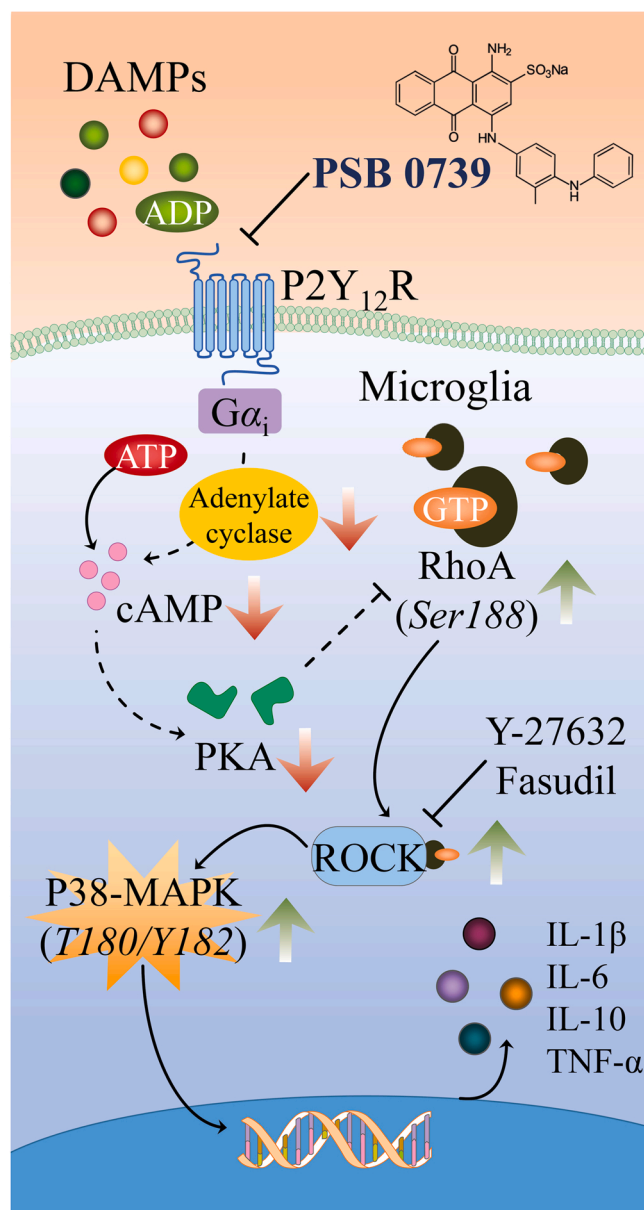

Fig. 7. Putative model of microglial $P2Y_{12}$-receptor and its downstream signalling mechanism during disease progression in Parkinson's disease Neurodegeneration during Parkinson's disease causes the release of damage-associated molecular pattern molecules (DAMPs), such as ADP and ATP. The released nucleotides active $P2Y_{12}$-receptor ($P2Y_{12}R$) expressed on microglia, and subsequently through activation of the heterotrimeric G protein Gi results in the inhibitory regulation of adenylate cyclase. Decreased levels of cAMP leads to reduced protein kinase A (PKA) activity, which in turn results in reduced phosphorylation of RhoA at serine 188. Phosphorylation of RhoA at serine 188 negatively regulate RhoA activity; therefore, the decreased phosphorylation state results in increased RhoA and in turn, enhanced ROCK and p38 MAPK activity, which then leads to bolstered pro- and anti-inflammatory cytokine biosynthesis. Arrows indicate stimulation, blunt lines represent inhibition, dashed line illustrate putative mechanism. Red arrows indicate decrease in concentration or activity, green arrows indicate increased enzymatic activity. PSB 0739 is a specific inhibitor of $P2Y_{12}R$, Y-27632 and fasudil are specific inhibitors for ROCK.

Andersen and colleagues [76], using summary statistics from recent meta-analysis genome-wide association studies in PD patients. They identified significant enrichment of PD risk heritability in microglia and monocytes and *P2RY12* was indicated as the strongest candidate gene driving a significant Parkinson's disease association signal. Their

finding, albeit lacking data, whether functionally relevant polymorphisms are identified in the proposed *P2RY12* candidate gene region; nevertheless corroborates our findings that neuroimmune mechanisms during PD pathogenesis as well as the apparent microglia dysregulation are strongly influenced by $P2Y_{12}R$ function in human patients.

5. Conclusions

A fundamental function of microglia is their ability to respond to harmful stimuli and trigger inflammatory response, while also to initiate disease resolution and neuroprotection. We have identified the G_i-coupled $P2Y_{12}$-receptor to sense the increased levels of nucleotides released during cellular damage, and to initiate cytokine production by regulating p38 MAPK activity via ROCK1. Blockade of $P2Y_{12}R$ is harmful in the acute phase of MPTP-induced Parkinsonism, presumably due to the impaired phagocytic activity of activated microglia; but prevents MPTP-induced dopaminergic neuron loss and the development of Parkinson's disease at later time points. Furthermore, inhibition of the receptor abrogates disease progression, reduces motor function impairment and mitigates neuronal cell death. Thus, understanding the complex mechanisms through which $P2Y_{12}R$ signalling in the CNS contributes to injury or repair may allow targeted modulation of microglial responses and neuroinflammation to shape disease progression during Parkinson's disease.

CRediT authorship contribution statement

Andras Iring: Conceptualization, Methodology, Validation, Formal analysis, Investigation, Writing – original draft, Writing – review & editing, Visualization. **Adrián Tóth:** Validation, Investigation, Writing – review & editing. **Mária Baranyi:** Methodology, Formal analysis, Investigation, Data curation, Writing – original draft. **Lilla Otrokocsi:** Validation, Investigation. **László V. Módis:** Investigation, Resources. **Flóra Gölöncsér:** Validation, Investigation, Writing – original draft, Visualization. **Bernadett Varga:** Investigation. **Tibor Hortobágyi:** Conceptualization, Methodology, Resources, Supervision, Writing – original draft. **Dániel Bereczki:** Conceptualization, Supervision, Writing – original draft. **Ádám Dénes:** Conceptualization, Methodology, Resources, Writing – original draft, Writing – review & editing, Supervision. **Beáta Sperlágh:** Conceptualization, Methodology, Data curation, Writing – original draft, Writing – review & editing, Visualization, Supervision, Project administration, Funding acquisition.

Declaration of Competing Interest

The authors declare that they have no known competing financial interests or personal relationships that could have appeared to influence the work reported in this paper.

Data Availability

Data will be made available upon reasonable request.

Acknowledgements

Appendix A. Supporting information

Supplementary data associated with this article can be found in the online version at doi:10.1016/j.phrs.2021.106045.

References

[1] J. Parkinson, An essay on the shaking palsy. 1817, J. Neuropsychiatry Clin. Neurosci. 14 (2) (2002) 223–236.
[2] D.K. Simon, C.M. Tanner, P. Brundin, Parkinson disease epidemiology, pathology, genetics, and pathophysiology, Clin. Geriatr. Med. 36 (1) (2020) 1–12.
[3] B. Pinter, A. Diem-Zangerl, G.K. Wenning, C. Scherfler, W. Oberaigner, K. Seppi, W. Poewe, Mortality in Parkinson's disease: a 38-year follow-up study, Mov. Disord. 30 (2) (2015) 266–269.
[4] E.R. Dorsey, T. Sherer, M.S. Okun, B.R. Bloem, The emerging evidence of the Parkinson pandemic, J. Parkinson's Dis. 8 (s1) (2018) S3–S8.
[5] K.A. Jellinger, Morphological substrates of parkinsonism with and without dementia: a retrospective clinico-pathological study, J. Neural Transm. 72 (2007) 91–104.
[6] K.A. Jacobson, E.G. Delicado, C. Gachet, C. Kennedy, I. von Kügelgen, B. Li, M. T. Miras-Portugal, I. Novak, T. Schöneberg, R. Perez-Sen, D. Thor, B. Wu, Z. Yang, C.E. Müller, Update of P2Y receptor pharmacology: IUPHAR review 27, Br. J. Pharmacol. 177 (11) (2020) 2413–2433.
[7] C.S. Moore, A.R. Ase, A. Kinsara, V.T. Rao, M. Michell-Robinson, S.Y. Leong, O. Butovsky, S.K. Ludwin, P. Seguela, A. Bar-Or, J.P. Antel, P2Y12 expression and function in alternatively activated human microglia, Neurol. Neuroimmunol. Neuroinflamm. 2 (2) (2015).
[8] N. Moskal, V. Riccio, M. Bashkurov, R. Taddese, A. Datti, P.N. Lewis, G. Angus, McQuibban. ROCK inhibitors upregulate the neuroprotective Parkin-mediated mitophagy pathway, Nat. Commun. 11 (1) (2020) 019–13781.
[9] K. Beko, B. Kovanyi, F. Goloncser, G. Horvath, A. Denes, Z. Kornyei, B. Botz, Z. Helyes, C.E. Muller, B. Sperlagh, Contribution of platelet P2Y12 receptors to chronic Complete Freund's adjuvant-induced inflammatory pain, J. Thromb. Haemost. 15 (6) (2017) 1223–1235.
[10] C. Cserep, B. Posfai, N. Lenart, R. Fekete, Z.I. Laszlo, Z. Lele, B. Orsolits, G. Molnar, S. Heindl, A.D. Schwarcz, K. Ujvari, Z. Kornyei, K. Toth, E. Szabadits, B. Sperlagh, M. Baranyi, L. Csiba, T. Hortobagyi, Z. Magloczky, B. Martinecz, G. Szabo, F. Erdelyi, R. Szipocs, M.M. Tamkun, B. Gesierich, M. Duering, I. Katona, A. Liesz, G. Tamas, A. Denes, Microglia monitor and protect neuronal function via specialized somatic purinergic junctions, Microcontact 367 (6477) (2020) 528–537.
[11] S.E. Haynes, G. Hollopeter, G. Yang, D. Kurpius, M.E. Dailey, W.B. Gan, D. Julius, The P2Y12 receptor regulates microglial activation by extracellular nucleotides, Nat. Neurosci. 9 (12) (2006) 1512–1519.
[12] G. Gelders, V. Baekelandt, A. Van der Perren, Linking neuroinflammation and neurodegeneration in Parkinson's disease, J. Immunol. Res. 16 (2018), 4784268.
[13] P.L. McGeer, S. Itagaki, B.E. Boyes, E.G. McGeer, Reactive microglia are positive for HLA-DR in the substantia nigra of Parkinson's and Alzheimer's disease brains, Neurology 38 (8) (1988) 1285–1291.
[14] C. Lambert, A.R. Ase, P. Seguela, J.P. Antel, Distinct migratory and cytokine responses of human microglia and macrophages to ATP, Brain Behav. Immun. 24 (8) (2010) 1241–1248.
[15] K. Williams, A. Bar-Or, E. Ulvestad, A. Olivier, J.P. Antel, V.W. Yong, Biology of adult human microglia in culture: comparisons with peripheral blood monocytes and astrocytes, J. Neuropathol. Exp. Neurol. 51 (5) (1992), 538-49.
[16] P.A. Lewitt, Levodopa for the treatment of Parkinson's disease, New Engl. J. Med. 359 (23) (2008) 2468–2476.
[17] C. Kilkenny, W. Browne, I.C. Cuthill, M. Emerson, D.G. Altman, Animal research: reporting in vivo experiments–the ARRIVE guidelines, J. Cereb. Blood Flow Metab. 31 (4) (2011) 991–993.
[18] J.C. McGrath, E. Lilley, Implementing guidelines on reporting research using animals (ARRIVE etc.): new requirements for publication in BJP (Epub), Br. J. Pharmacol. 2015 Jul. 172 (13) (2015 12) 3189–3193, https://doi.org/10.1111/bph.12955.
[19] G. Horvath, F. Goloncser, C. Csolle, K. Kiraly, R.D. Ando, M. Baranyi, B. Kovanyi, Z. Mate, K. Hoffmann, I. Algaier, Y. Baqi, C.E. Muller, I. Von Kugelgen, B. Sperlagh, Central P2Y12 receptor blockade alleviates inflammatory and neuropathic pain and cytokine production in rodents, Neurobiol. Dis. 70 (2014), 162-78.
[20] M. Baranyi, P.F. Porceddu, F. Goloncser, S. Kulcsar, L. Otrokocsi, A. Kittel, A. Pinna, L. Frau, P.B. Huleatt, M.L. Khoo, C.L. Chai, P. Dunkel, P. Matyus, M. Morelli, B. Sperlagh. Novel (Hetero)arylalkenyl propargylamine compounds are protective in toxin-induced models of Parkinson's disease, Mol. Neurodegener. 11 (6) (2016) 015–0067.
[21] C. Mestre, T. Pélissier, J. Fialip, G. Wilcox, A. Eschalier, A method to perform direct transcutaneous intrathecal injection in rats, J. Pharm. Toxicol. Methods 32 (4) (1994) 197–200.
[22] Y. Baqi, K. Atzler, M. Köse, M. Glänzel, C.E. Müller, High-affinity, non-nucleotide-derived competitive antagonists of platelet P2Y12 receptors, J. Med. Chem. 52 (12) (2009) 3784–3793.
[23] H. Shiotsuki, K. Yoshimi, Y. Shimo, M. Funayama, Y. Takamatsu, K. Ikeda, R. Takahashi, S. Kitazawa, N. Hattori, A rotarod test for evaluation of motor skill learning, J. Neurosci. Methods 189 (2) (2010) 180–185.

[24] C.W. Ip, D. Cheong, J. Volkmann, Stereological estimation of dopaminergic neuron number in the mouse substantia nigra using the optical fractionator and standard microscopy equipment, J. Vis. Exp. 1 (127) (2017) 56103.

[25] M.J. West, L. Slomianka, H.J. Gundersen, Unbiased stereological estimation of the total number of neurons in thesubdivisions of the rat hippocampus using the optical fractionator, Anat. Rec. 231 (4) (1991) 482–497.

[26] J.I. Keuker, G.K. Vollmann-Honsdorf, E. Fuchs, How to use the optical fractionator: an example based on the estimation of neurons in the hippocampal CA1 and CA3 regions of tree shrews, Brain Res. Protoc. 7 (3) (2001), 211-21.

[27] A. Lopez-Lopez, C.M. Labandeira, J.L. Labandeira-Garcia, A. Muñoz, A. Rho kinase inhibitor fasudil reduces l-DOPA-induced dyskinesia in a rat model of Parkinson's disease, Br. J. Pharmacol. 28 (10) (2020) 15275.

[28] C.A. Paul, B. Beltz, J. Berger-Sweeney, The nissl stain: a stain for cell bodies in brain sections, CSH Protoc. 1 (10) (2008).

[29] M.H. Shihan, S.G. Novo, S.J. Le Marchand, Y. Wang, M.K. Duncan, A simple method for quantitating confocal fluorescent images, Biochem. Biophys. Rep. 25 (100916) (2021).

[30] O.H. Lowry, N.J. Rosebrough, A.L. Farr, R.J. Randall, Protein measurement with the Folin phenol reagent, J. Biol. Chem. 193 (1) (1951), 265-75.

[31] M. Baranyi, E. Milusheva, E.S. Vizi, B. Sperlagh, Chromatographic analysis of dopamine metabolism in a Parkinsonian model, J. Chromatogr. A 7 (2006) 1–2.

[32] K.Z. Chapman, V.Q. Dale, A. Denes, G. Bennett, N.J. Rothwell, S.M. Allan, B.W. McColl. A rapid and transient peripheral inflammatory response precedes brain inflammation after experimental stroke, J. Cereb. Blood Flow Metab. 29 (11) (2009) 1764–1768.

[33] A. Denes, N. Humphreys, T.E. Lane, R. Grencis, N. Rothwell, Chronic systemic infection exacerbates ischemic brain damage via a CCL5 (regulated on activation, normal T-cell expressed and secreted)-mediated proinflammatory response in mice, J. Neurosci. 30 (30) (2010), 10086-95.

[34] B. Kovanyi, C. Csolle, A. Calovi, A. Hanuska, E. Kato, L. Koles, A. Bhattacharya, J. Haller, B. Sperlagh, The role of P2×7 receptors in a rodent PCP-induced schizophrenia model, Sci. Rep. 6 (2016) 36680.

[35] R. Skogseth, T. Hortobagyi, H. Soennesyn, L. Chwiszczuk, D. Ffytche, A. Rongve, C. Ballard, D. Aarsland, Accuracy of clinical diagnosis of dementia with lewy bodies versus neuropathology, J. Alzheimers Dis. 59 (4) (2017) 1139–1152.

[36] J. Charan, T.Biswas How to calculate sample size for different study designs in medical research? Indian J. Psychol. Med. 35 (2) (2013) 121–126.

[37] K. Hoffmann, Y. Baqi, M.S. Morena, M. Glanzel, C.E. Muller, I. von Kugelgen, Interaction of new, very potent non-nucleotide antagonists with Arg256 of the human platelet P2Y12 receptor, J. Pharmacol. Exp. Ther. 331 (2) (2009) 648–655.

[38] N. Charolidi, T. Schilling, C. Eder, Microglial Kv1.3 channels and P2Y12 receptors differentially regulate cytokine and chemokine release from brain slices of young adult and aged mice, PLoS One 10 (5) (2015).

[39] D.G. Walker, T.M. Tang, A. Mendsaikhan, I. Tooyama, G.E. Serrano, L.I. Sue, T. G. Beach, L.F. Lue, Patterns of expression of purinergic receptor P2RY12, a putative marker for non-activated microglia, in aged and Alzheimer's disease brains, Int. J. Mol. Sci. 21 (2) (2020).

[40] R.A. Gottlieb, Programmed cell death, Drug N. Perspect. 13 (8) (2000) 471–476.

[41] S. Ghavami, M. Hashemi, S.R. Ande, B. Yeganeh, W. Xiao, M. Eshraghi, C.J. Bus, K. Kadkhoda, E. Wiechec, A.J. Halayko, M. Los, Apoptosis and cancer: mutations within caspase genes, J. Med. Genet. 46 (8) (2009) 497–510.

[42] N. Gresa-Arribas, C. Viéitez, G. Dentesano, J. Serratosa, J. Saura, C. Solà, Modelling neuroinflammation in vitro: a tool to test the potential neuroprotective effect of anti-inflammatory agents, PLoS One 7 (9) (2012) 20.

[43] M. Gaestel, MAPKAP kinases - MKs - two's company, three's a crowd, Nat. Rev. Mol. Cell Biol. 7 (2) (2006) 120–130.

[44] A.D. Bachstetter, L.J. Van Eldik, The p38 MAP kinase family as regulators of proinflammatory cytokine production in degenerative diseases of the CNS, Aging Dis. 1 (3) (2010) 199–211.

[45] C. Kim, Y. Sano, K. Todorova, B.A. Carlson, L. Arpa, A. Celada, T. Lawrence, K. Otsu, J.L. Brissette, J.S. Arthur, J.M. Park, The kinase p38 alpha serves cell type-specific inflammatory functions in skin injury and coordinates pro- and anti-inflammatory gene expression, Nat. Immunol. 9 (9) (2008) 1019–1027.

[46] A.P. de Souza, V.L. Vale, C. Silva Mda, I.B. Araujo, S.C. Trindade, L.F. de Moura-Costa, G.C. Rodrigues, T.S. Sales, H.A. dos Santos, P.C. de Carvalho-Filho, M.G. de Oliveira-Neto, R.E. Schaer, R. Meyer, MAPK involvement in cytokine production in response to Corynebacterium pseudotuberculosis infection, BMC Microbiol. 14 (230) (2014) 014–0230.

[47] A. Cuenda, S. Rousseau, p38 MAP-kinases pathway regulation, function and role in human diseases, Biochim. Biophys. Acta 8 (75) (2007) 24.

[48] E. Tatsumi, H. Yamanaka, K. Kobayashi, H. Yagi, M. Sakagami, K. Noguchi, RhoA/ROCK pathway mediates p38 MAPK activation and morphological changes downstream of P2Y12/13 receptors in spinal microglia in neuropathic pain, Glia 63 (2) (2015), 216-28.

[49] J. Albarrán-Juárez, A. Iring, S. Wang, S. Joseph, M. Grimm, B. Strilic, N. Wettschureck, T.F. Althoff, S. Offermanns, Piezo1 and G(q)/G(11) promote endothelial inflammation depending on flow pattern and integrin activation, J. Exp. Med. 215 (10) (2018) 2655–2672.

[50] D.G. Walker, L.F. Lue, Immune phenotypes of microglia in human neurodegenerative disease: challenges to detecting microglial polarization in human brains, Alzheimers Res. Ther. 7 (1) (2015) 015–0139.

[51] R.T. Dorsam, S.P. Kunapuli, Central role of the P2Y12 receptor in platelet activation, J. Clin. Investig. 113 (3) (2004) 340–345.

[52] O. Butovsky, M.P. Jedrychowski, C.S. Moore, R. Cialic, A.J. Lanser, G. Gabriely, T. Koeglsperger, B. Dake, P.M. Wu, C.E. Doykan, Z. Fanek, L. Liu, Z. Chen, J. D. Rothstein, R.M. Ransohoff, S.P. Gygi, J.P. Antel, H.L. Weiner, Identification of a unique TGF-β-dependent molecular and functional signature in microglia, Nat. Neurosci. 17 (1) (2014) 131–143.

[53] H. Franke, U. Krügel, J. Grosche, C. Heine, W. Härtig, C. Allgaier, P. Illes, P2Y receptor expression on astrocytes in the nucleus accumbens of rats, Neuroscience 127 (2) (2004) 431–441.

[54] R.D. Hodge, T.E. Bakken, J.A. Miller, K.A. Smith, E.R. Barkan, L.T. Graybuck, J. L. Close, B. Long, N. Johansen, O. Penn, Z. Yao, J. Eggermont, T. Hollt, B.P. Levi, S. I. Shehata, B. Aevermann, A. Beller, D. Bertagnolli, K. Brouner, T. Casper, C. Cobbs, R. Dalley, N. Dee, S.L. Ding, R.G. Ellenbogen, O. Fong, E. Garren, J. Goldy, R. P. Gwinn, D. Hirschstein, C.D. Keene, M. Keshk, A.L. Ko, K. Lathia, A. Mahfouz, Z. Maltzer, M. McGraw, T.N. Nguyen, J. Nyhus, J.G. Ojemann, A. Oldre, S. Parry, S. Reynolds, C. Rimorin, N.V. Shapovalova, S. Somasundaram, A. Szafer, E. R. Thomsen, M. Tieu, G. Quon, R.H. Scheuermann, R. Yuste, S.M. Sunkin, B. Lelieveldt, D. Feng, L. Ng, A. Bernard, M. Hawrylycz, J.W. Phillips, B. Tasic, H. Zeng, A.R. Jones, C. Koch, E.S. Lein, Conserved cell types with divergent features in human versus mouse cortex, Nature 573 (7772) (2019) 61–68.

[55] S. Amadio, G. Tramini, A. Martorana, M.T. Viscomi, G. Sancesario, G. Bernardi, C. Volonté, Oligodendrocytes express P2Y12 metabotropic receptor in adult rat brain, Neuroscience 141 (3) (2006) 1171–1180.

[56] A. Nimmerjahn, F. Kirchhoff, F. Helmchen, Resting microglial cells are highly dynamic surveillants of brain parenchyma in vivo, Science 308 (5726) (2005) 1314–1318.

[57] D. Boche, V.H. Perry, J.A. Nicoll, Review: activation patterns of microglia and their identification in the human brain, Neuropathol. Appl. Neurobiol. 39 (1) (2013) 3–18.

[58] E.E. Benarroch, Microglia: multiple roles in surveillance, circuit shaping, and response to injury, Neurology 81 (12) (2013) 1079–1088.

[59] S.R. Subramaniam, H.J. Federoff, Targeting microglial activation states as a therapeutic avenue in Parkinson's disease, Front. Aging Neurosci. 9 (176) (2017).

[60] K. Imamura, N. Hishikawa, M. Sawada, T. Nagatsu, M. Yoshida, Y. Hashizume, Distribution of major histocompatibility complex class II-positive microglia and cytokine profile of Parkinson's disease brains, Acta Neuropathol. 106 (6) (2003) 518–526.

[61] P. Illes, P. Rubini, H. Ulrich, Y. Zhao, Y. Tang, Regulation of microglial functions by purinergic mechanisms in the healthy and diseased CNS, Cells 9 (5) (2020).

[62] X. Yang, H. Ren, K. Wood, M. Li, S. Qiu, F.D. Shi, C. Ma, Q. Liu, Depletion of microglia augments the dopaminergic neurotoxicity of MPTP, FASEB J. 32 (6) (2018) 3336–3345.

[63] L. Tönges, T. Frank, L. Tatenhorst, K.A. Saal, J.C. Koch, M. Szego É, M. Bähr, J. H. Weishaupt, P. Lingor, Inhibition of rho kinase enhances survival of dopaminergic neurons and attenuates axonal loss in a mouse model of Parkinson's disease, Brain 135 (11) (2012) 3355–3370.

[64] R. Fekete, C. Cserep, N. Lenart, K. Toth, B. Orsolits, B. Martinecz, E. Mehes, B. Szabo, V. Nemeth, B. Gonci, B. Sperlagh, Z. Boldogkoi, A. Kittel, M. Baranyi, S. Ferenczi, K. Kovacs, G. Szalay, B. Rozsa, C. Webb, G.G. Kovacs, T. Hortobagyi, B. L. West, Z. Kornyei, A. Denes, Microglia control the spread of neurotropic virus infection via P2Y12 signalling and recruit monocytes through P2Y12-independent mechanisms, Acta Neuropathol. 136 (3) (2018) 461–482.

[65] P. Swiatkowski, M. Murugan, U.B. Eyo, Y. Wang, S. Rangaraju, S.B. Oh, L.J. Wu, Activation of microglial P2Y12 receptor is required for outward potassium currents in response to neuronal injury, Neuroscience 318 (2016) 22–33.

[66] D. Davalos, J. Grutzendler, G. Yang, J.V. Kim, Y. Zuo, S. Jung, D.R. Littman, M. L. Dustin, W.B. Gan, ATP mediates rapid microglial response to local brain injury in vivo, Nat. Neurosci. 8 (6) (2005) 752–758.

[67] K. Ohsawa, Y. Irino, Y. Nakamura, C. Akazawa, K. Inoue, S. Kohsaka, Involvement of P2×4 and P2Y12 receptors in ATP-induced microglial chemotaxis, Glia 55 (6) (2007) 604–616.

[68] T. Yu, X. Zhang, H. Shi, J. Tian, L. Sun, X. Hu, W. Cui, D. Du, P2Y12 regulates microglia activation and excitatory synaptic transmission in spinal lamina II neurons during neuropathic pain in rodents, Cell Death Dis. 10 (3) (2019) 019–1425.

[69] J. Raingeaud, S. Gupta, J.S. Rogers, M. Dickens, J. Han, R.J. Ulevitch, R.J. Davis Pro-inflammatory, cytokines and environmental stress cause p38 mitogen-activated protein kinase activation by dual phosphorylation on tyrosine and threonine, J. Biol. Chem. 270 (13) (1995) 7420–7426.

[70] J. Han, J.D. Lee, L. Bibbs, R.J. Ulevitch, A MAP kinase targeted by endotoxin and hyperosmolarity in mammalian cells, Science 265 (5173) (1994) 808–811.

[71] N.W. Freshney, L. Rawlinson, F. Guesdon, E. Jones, S. Cowley, J. Hsuan, J. Saklatvala, Interleukin-1 activates a novel protein kinase cascade that results in the phosphorylation of Hsp27, Cell 78 (6) (1994) 1039–1049.

[72] H. Scheiblich, G. Bicker, Regulation of microglial phagocytosis by RhoA/ROCK-inhibiting drugs, Cell Mol. Neurobiol. 37 (3) (2017) 461–473.

[73] J.C. Koch, L. Tatenhorst, A.E. Roser, K.A. Saal, L. Tönges, P. Lingor, ROCK inhibition in models of neurodegeneration and its potential for clinical translation, Pharmacol. Ther. 189 (2018) 1–21.

[74] L. Tatenhorst, L. Tönges, K.A. Saal, J.C. Koch, M. Szegő É, M. Bähr, P. Lingor, Rho kinase inhibition by fasudil in the striatal 6-hydroxydopamine lesion mouse model of Parkinson disease, J. Neuropathol. Exp. Neurol. 73 (8) (2014) 770–779.

[75] R. Guo, B. Liu, S. Zhou, B. Zhang, Y. Xu, The protective effect of fasudil on the structure and function of cardiac mitochondria from rats with type 2 diabetes induced by streptozotocin with a high-fat diet is mediated by the attenuation of oxidative stress, Biomed. Res. Int. 430791 (10) (2013) 22.

[76] M.S. Andersen, S. Bandres-Ciga, R.H. Reynolds, J. Hardy, M. Ryten, L. Krohn, Z. Gan-Or, I.R. Holtman, L. Pihlstrøm, Heritability enrichment implicates microglia in Parkinson's disease pathogenesis, Ann. Neurol. 27 (10) (2021) 26032.